PREDICTING THE MOTIONS OF DETACHED ICE FLOES

by

URI FELDMAN, M.Sc.

A Thesis

Submitted to the School of Graduate Studies

in Partial Fulfilment of the Requirements

for the Degree

Doctor of Philosophy

McMaster University

August, 1978

#1

PREDICTING THE MOTIONS OF DETACHED ICE FLOES

DOCTOR OF PHILOSOPHY (1978) McMASTER UNIVERSITY

(Geography) Hamilton, Ontario

TITLE: Predicting the Motions of Detached Ice Floes

AUTHOR: Uri Feldman, M.Sc. (Hebrew University of Jerusalem)

SUPERVISOR: Professor P.U. Howarth

NUMBER OF PAGES: 144, XIV

ABSTRACT

Methods for predicting motions of drifting open pack ice and determining wind fields and ice parameters, associated with these motions, are needed for studying sea ice dynamics in the Polar Oceans. The new ice motion prediction method, developed and tested in this study, is a response to these needs. To ensure its applicability only readily available data, such as surface weather charts and LANDSAT-1 MSS images, were used. The method is able

a. to predict the motions of groups of wind driven detached ice floes over periods of 12, 36 and 60 hours.

b. to determine the surface wind fields, sea ice thickness and the surface and subsurface drag coefficients associated with these motions. This did not require any ice based measurements.

The method was developed by assuming wind stress, water drag and Coriolis force to be at equilibrium for a drifting group. Parameters associated with these motions were obtained from three day data sequences. Surface wind speed was estimated from the geostrophic wind fields, obtained from surface weather charts. Ice motion velocity was calculated from LANDSAT-1 MSS images. The angle of sea ice deflection, the cross isobar angles, sea ice thickness and the surface and subsurface drag coefficients were determined by solving the equilibrium equation of motion for detached ice floes, using values of the minima, maxima, means and ratios of these parameters. Weather data from a fourth day were used to predict the motions for this day. Where available, LANDSAT-1 MSS images for this day were used to test these predictions.

The method has practical usefulness if used in conjunction with data from microwave sensing systems. The predictions and parameters could be applied to support marine traffic and exploration of natural resources in the Polar Oceans. Wind fields and sea ice parameters, which were formerly practically unavailable can now be derived by the method. The knowledge gained in this study can lead to a better understanding of the physical environment in the Polar Oceans.

ACKNOWLEDGEMENTS

I wish to express my deep appreciation to Professor P.J. Howarth, who supervised this research, for his inspiring guidance and generous support and for the knowledge gained from him throughout the course of my studies. I am sincerely indebted to Professor J.A. Davies for his helpful counsel and for graciously giving of his time to read and constructively comment upon the drafts. Thanks are due to Professor H.P. Schwarcz for critically reviewing the manuscript and to Professor S.B. McCann for his helpful advice. I am grateful to Professor M-k. Woo for his continuous interest in the progress of the study; to Dr. Z. Drezner and Dr. D. Nir for their helpful suggestions and critical comments; to Mrs. N.J. Kozlovic for her excellent assistance in the remote sensing laboratory and to Mrs. A.M. Kimmel for her skill and speed in typing the manuscript. My gratitude extends also to friends and colleagues at McMaster University and the Atmospheric Environment Service for their generous help and constant encouragement.

Finally, my heartiest thanks go to Edna, my wife, for her patience and understanding and to our sons, who can now go back to making noise at home.

TABLE OF CONTENTS

TABLE OF CONTENTS (Cont'd)

TABLE OF CONTENTS (Cont'd)

LIST OF ILLUSTRATIONS

LIST OF TABLES

CHAPTER 1

INTRODUCTION

1.1 Purpose of Study

The motions of groups of detached ice floes are determined and predicted for periods of 12, 36 and 60 hours. Surface wind fields, sea ice thickness, surface drag coefficient and subsurface drag coefficient associated with these motions are calculated. The prediction method uses only readily available data, such as surface weather charts and LANDSAT-1 MSS images.

1.2 Area of Study

The area of study was selected from zones where detached ice floes drift along the edge of the close pack ice*. The south east sector of the Beaufort Sea, west of Baillie Island (Northwest Territories) and east of Barter Island (Alaska), between the parallels 69°N and 71°N was selected as a suitable area (Figure 1.1). Local influences, such as those affecting sea ice around the islands of the Canadian Arctic Archipelago are minimized. At these latitudes the orbital paths of LANDSAT-1, which converge polewards, provide sequences of four sidelapping images. Ice floes displacements were measured on sequential images from fixed points on land. The accuracy of these measurements is inversely related to the distance from land. Therefore,

---

* Pack ice in which the concentration is 10/10 and no water is visible (WMO, 1972).

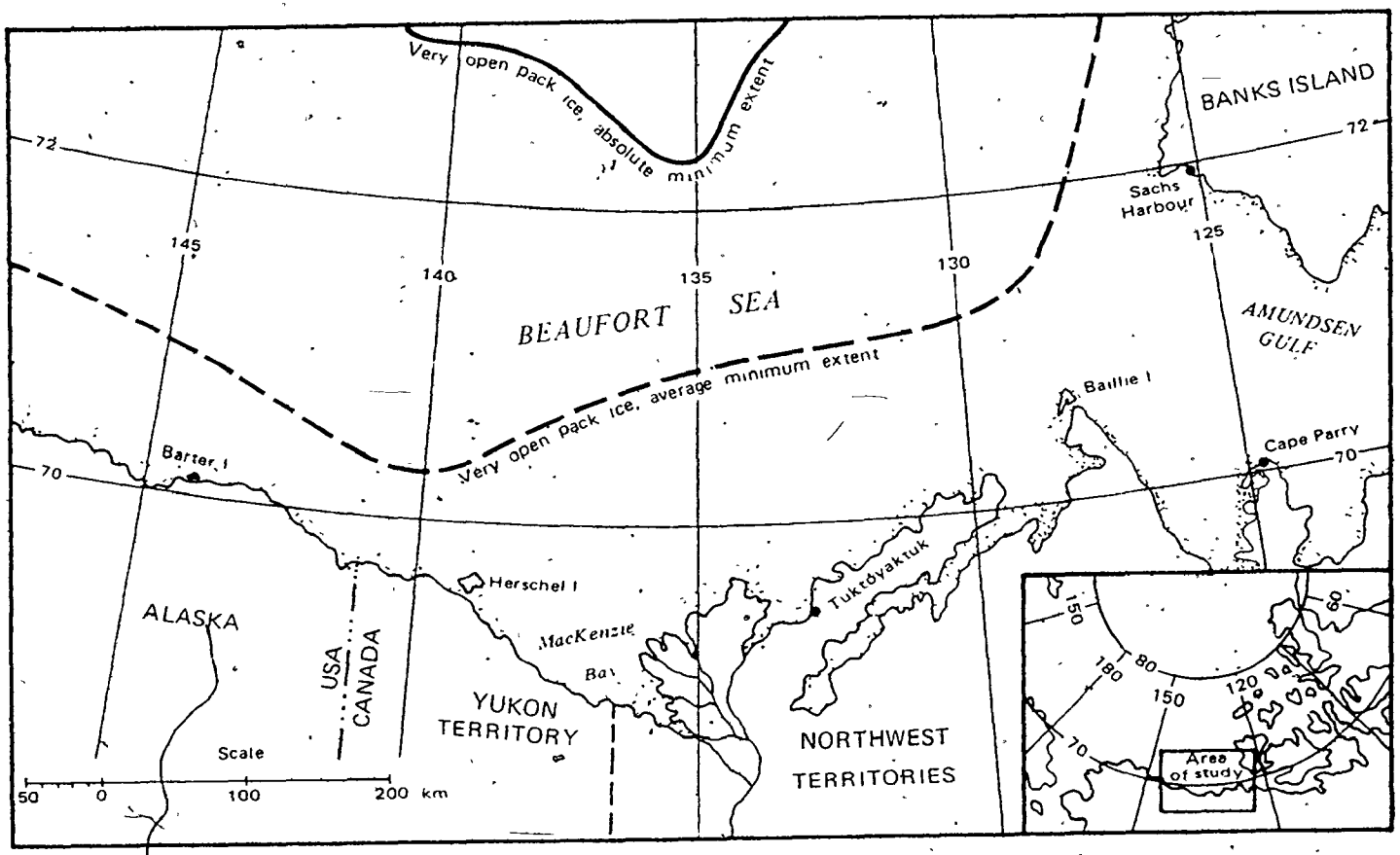

Figure 1.1 Extent of very open pack ice during summer at the area of study (AGS, 1975)

groups of ice floes located farther than 400 km from land were not considered.

1.3 Physical Background

It is generally agreed that motions of drifting pack ice result mainly from the action of five forces (Campbell, 1965; Maykut, Thorndike and Untersteiner, 1972; Coon, 1977). Following Campbell (1965) the general equation of motion for a unit area of drifting compact pack ice can be written as

$$\vec{\tau}_a + \vec{\tau}_w + \vec{C} + \vec{P} + \vec{I} = \rho_{ice} h \, d\vec{V}/dt \qquad (1.1)$$

where $\vec{\tau}_a$ is the horizontal air stress at the air/ice interface, $\vec{\tau}_w$ the horizontal water stress at the water/ice interface, $\vec{C}$ the horizontal Coriolis deflecting force; $\vec{P}$ the horizontal marine pressure gradient stress, is generated and controlled by the general atmospheric circulation over the ocean basin, by the configuration of its shores and by water exchange with neighbouring basins (Fel'zenbaum, 1958); $\vec{I}$ the internal ice stress, is generated by the resultant of the above mentioned stresses, acting elsewhere in the basin and transmitted through the compact pack ice; ρ_{ice} the ice density, h the ice thickness, and $d\vec{V}/dt$ the ice acceleration. Most studies on the motions of ice assume that acceleration is negligible (Nansen, 1902; Sverdrup, 1928; Rossby and Montgomery, 1935; Fel'zenbaum, 1958; Reed and Campbell, 1960; Campbell, 1965 and Neralla et al., 1977). Thorndike (1973) has shown that the acceleration term is generally

much smaller than the other terms in equation (1.1) and that this assumption is, therefore, valid. For a steady state drift of sea ice the most general form of the equation of motion is

$$\vec{\tau}_a + \vec{\tau}_w + \vec{C} + \vec{P} + \vec{I} = 0 \qquad (1.2)$$

Equation (1.2) may be simplified for short periods of time (less than 60 hours) and for detached ice floes. Under these conditions $\vec{P} \simeq 0$ (Post, 1954) and $\vec{I} = 0$, because $\vec{I}$ can be transmitted only through compact pack ice (Untersteiner, 1977). With these assumptions equation (1.2) reduces to

$$\vec{\tau}_a + \vec{\tau}_w + \vec{C} = 0 \qquad (1.3)$$

This equation was first suggested and used by Nansen (1902) and later applied by Shuleiken (1938), Reed and Campbell (1962) and Neralla et al. (1977). It is used in this study. Values of τ_a, τ_w and C may be obtained by assuming that under conditions of neutral equilibrium within the atmospheric surface boundary layer

$$\tau_a = \rho_a C_d^a U^2 \qquad (1.4)$$

(McIntosh and Thom, 1972), where ρ_a is the air density,

C_d^a the drag coefficient at the air/ice interface and U the horizontal surface wind speed at 10 m above the ice surface. Under similar conditions beneath the ice (Johannessen, 1970)

$$\tau_w = \rho_w C_d^w V^2 \qquad (1.5)$$

where ρ_w is the ocean water density, C_d^w is the drag coefficient at the water-ice interface and V is the speed of the centre of gravity of a drifting group of ice floes. The values of C may be obtained from

$$C = \rho_{ice} f h V \qquad (1.6)$$

where f (= $2\omega \sin \phi$) is the Coriolis parameter, ω (= $7.292\ 10^{-5} s^{-1}$) is the Earth's angular speed and ϕ is latitude. The stress vectors τ_a, τ_w and C and the velocity vectors U and V at equilibrium are shown in Figure 1.2. θ_U and θ_{ice} are the directions of the surface wind and the ice motion respectively.

Procedures used to determine the geostrophic wind speed G and direction θ_G and to obtain the values of eight unknown parameters in equations (1.4), (1.5) and (1.6), are presented in Chapters 2 - 4. Those dealing with G, θ_G, ρ_a, U, V and θ_{ice} are discussed in Chapters 2 and 3. Since θ_U cannot be determined directly from the available wind fields it was replaced by the angle of sea ice deflection $\Delta\gamma$, defined as

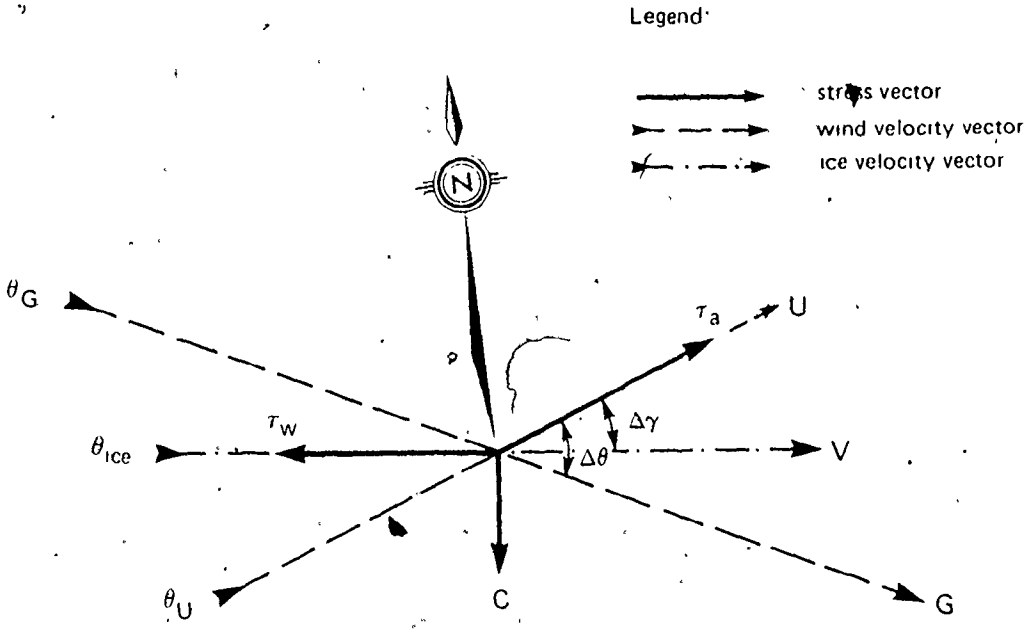

Figure 1.2 Arrangement of vectors at equilibrium

$$\Delta\gamma = \theta_{ice} - \theta_U \tag{1.7}$$

and by the cross isobar angle $\Delta\theta$ (Figure 1.2), defined as

$$\Delta\theta = \theta_G - \theta_U \tag{1.8}$$

Procedures employed to determine the values of $\Delta\gamma$, $\Delta\theta$, h, C_d^a and C_d^w and to predict the motions of groups of detached ice floes, are presented in Chapter 4.

CHAPTER 2

ESTIMATES OF THE SURFACE WIND FROM THE GEOSTROPHIC WIND APPROXIMATION

2.1 Geostrophic Wind Fields from Surface Weather Charts

The geostrophic wind approximates the horizontal wind at the top of the planetary boundary layer above the influence of surface friction. It results from the balance between the Coriolis acceleration and the horizontal pressure force. Speed of the geostrophic wind was calculated from the charts by the geostrophic wind equation (Hess, 1959) written as

$$G = (1/\rho_a f)(dp/dn) \qquad (2.1)$$

where p is the atmospheric pressure, n the horizontal distance measured normal to the isobars and dp/dn the horizontal pressure gradient. Differentials were replaced by finite differences and a fixed value of 0.4kPa was used for dp. Air density was determined from

$$\rho_a = p/R_d T_a \qquad (2.2)$$

where R_d is the gas constant for dry air (R_d = 2.87 10^2 J kg^{-1} $^0K^{-1}$) and T_a air temperature in ^0K. Geostrophic wind direction which is parallel to the isobars, with low pressure to the left, was obtained directly from the charts.

2.2 Relationship between Surface and Geostrophic Winds

In the absence of local and advective acceleration of motion the difference between surface and geostrophic wind velocities arises from the frictional drag exerted by the surface. The difference between the two velocities, although poorly understood, is determined by latitude, the surface drag coefficient, wind speed and atmospheric stability* in the planetary boundary layer (Roll, 1965).

Drag coefficient data and atmospheric stability were not available for the area during the period of study. Consequently, studies in which the relationships between $\vec{U}$ and $\vec{G}$ had been determined empirically were then evaluated for application. These relationships were previously obtained only over land and sea surfaces, but not over sea ice surfaces. Those obtained over sea surfaces were assumed to be applicable to sea ice surfaces for several reasons: firstly, the study area contains large stretches of open water; secondly, drag coefficients measured over sea surfaces are similar to those measured over sea ice surfaces (compare Roll, 1965 p. 158 with Tables 2.3 in this study). On the other hand, measurements of this parameter over land surfaces differ from those measured over sea ice surfaces by up to 5 orders of magnitude (McIntosh and Thom, 1972 p. 169).

Results from empirical studies on the relationships between surface and geostrophic wind speeds and wind directions are presented in Table 2.1. Aagaard (1969) correlated the relationship between the speed of the surface wind and

---

*A measure of the buoyant acceleration that would be acquired by an air parcel displaced vertically, in an atmosphere with known thermal stratification and moisture content.

TABLE 2.1

Relationship between Surface and Geostrophic Winds over Sea

No. of Observ.	Lat. °N	Relation of U to G		Cross Isobar Angle Δθ		References
		Range	mean	Range	mean	
-	5-55	0.40-0.88	-	35 - 13	-	Gordon, 1952
-	-	0.50	-	26 - 2	-	Reynolds, 1956
1460	66	0.94-1.28	1.05	22 - 11	17	Aagaard, 1969
438	54	*	-	-	-	Hásse and Wagnér, 1971
1460	54	*	-	20 - 10	-	Hasse, 1974a
1440	54	*	-	22 - 8	17.2	Hasse, 1974b
-	60	0.47-0.79	-	30 - 13	-	Lavrov, 1974
Summary of Results		0.40-1.28	-	35 - 2	-	

* determined from a linear equation

the speed of the geostrophic wind with atmospheric stability and associated extremely high values of the ratios (Table 2.1) with unstable conditions*. Hasse and Wagner (1971) first suggested that this relationship should be approximated by a linear equation of the form $U = aG + b$ where the slope coefficient a and the intercept b are calculated independently for unstable, near-neutral** and stable*** conditions. Values of a vary with latitude, and those of b with both latitude and atmospheric stability. Hasse defined stability by ΔT, the difference between air temperature T_a and sea surface temperature T_w. Values of b were calculated for three specific values of ΔT, namely: $\Delta T = -2.7$, -0.2 and $1.7^{\circ}C$ representing respectively unstable, near-neutral and stable atmospheric conditions. The coefficients a and b were amended by Hasse (1974a, 1974b) following further measurements, which provided a larger and more varied set of data. He concluded that the dependence of a and b on ΔT indicates that the relationship between U and G varies linearly with stability. Lavrov (1974) suggested that both stability and G determine the ratio between U and G.

According to Gordon (1952) the cross isobar angle

---

*Under unstable conditions in the atmosphere a displaced air parcel would be subjected to a buoyant acceleration acting in the direction of the displacement.

**Under near-neutral conditions in the atmosphere a displaced air parcel would experience no buoyant acceleration.

***Under stable conditions in the atmosphere a displaced air parcel would be subjected to a buoyant force opposite to its displacement.

is inversely related to the sine of the latitude (Table 2.1). Lavrov (1974) suggested that values of $\Delta\theta$ depend on atmospheric stability and are inversely related to the ratio between U and G. Hasse (1974b) showed that $\Delta\theta$ is controlled by atmospheric stability. He obtained lower values of $\Delta\theta$ under near-neutral stability and higher values under stable or unstable conditions.

2.3 Reliability of Calculations from Surface Weather Charts

If it can be shown that U, observed over sea ice, is linearly related to G, calculated from the charts, then, following Hasse's work, it may be inferred that the charts are a reliable source for G. The deviation of θ_G from θ_U is caused by the same frictional drag that causes the deviation of U from G and therefore it is assumed that the relationship between θ_G and θ_U is linear; thus if it can be shown that the relationship between θ_G, measured from the charts, and θ_U, observed over sea ice, is linear, then it can be inferred that the charts are also a reliable source of θ_G.

Observations conducted by Smith, Banke and Johannessen (1970), Smith (1972), Banke and Smith (1971), and Banke and Smith (1973) at six sites over sea ice provided the source for U and θ_U (Table 2.2). From these data, 81 out of 133 observations of wind speed and 61 out of 77 observations of wind direction were used. Data were rejected if they were incomplete or if isobaric patterns precluded reliable measurements of the geostrophic wind velocity. Surface weather charts for 0000, 0600, 1200 and 1800 G.M.T., compiled by AES* provided the source for the

*Atmospheric Environment Service, Canada

TABLE 2.2

Location, Number, Date and Source of Data Observed at the Sites

Site No.	Location	Lat. °N	Long. °W	No. of Observations W. Speed Coll.	W. Speed Used	W. Direc. Coll.	W. Direc. Used	Date	Data Source
1	Gulf of St. Lawrence	48	64	9	5	9	5	20.2.69	Smith, Banke and Johannessen, 1970
2	Gulf of St. Lawrence	47	63	56	20	-	-	6-23.3.70	Smith, 1972
3	Beaufort Sea	70	131	3	-	3	-		Banke and Smith, 1971
4a	Beaufort Sea (AIDJEX)	74	131	9	9	9	9	30.3- 2.4.71	Banke and Smith, 1973
4b	Beaufort Sea (AIDJEX)	74	131	8	7	8	7	5- 7.5.71	Banke and Smith, 1973
5	Arctic Ocean (AIDJEX)	75	150	30	24	30	24	30.3-18.4.72	Banke and Smith, 1973
6	Robeson Channel	82	60	18	16	18	16	19-23.7.72	Banke and Smith, 1973

TABLE 2.3

Observed and Calculated Wind Field Parameters

			Observed					Calculated	
Site No.*	Date	GMT	U $m\ s^{-1}$	θ_U Deg.	z/L -	T_a ^0K	$10^3 C_d^a$ -	G $m\ s^{-1}$	θ_G Deg.
1	20.2.69	1508	8.3	8	0.0004	274	2.73	7.8	72
	20.2.69	1643	8.0	10	0.0006	275	2.37	6.8	70
	20.2.69	1739	8.6	5	0.0003	276	2.62	6.1	69
	20.2.69	1825	9.5	8	0.0003	276	2.62	6.0	69
	20.2.69	1959	10.0	25	0.0003	275	2.88	6.3	72
2	6.3.70	1903	7.7	-	-0.004	271	1.36	7.5	28
	6.3.70	2111	7.0	-	0.002	268	2.14	7.0	24
	6.3.70	2302	8.4	-	-0.002	268	1.87	6.5	20
	6.3.70	2343	7.8	-	0.001	268	2.02	6.4	19
	10.3.70	1448	7.5	-	-0.008	264	1.43	8.9	279
	11.3.70	2338	6.7	-	-0.007	267	1.23	12.5	290
	12.3.70	1738	9.7	-	0.005	267	1.12	11.4	290
	13.3.70	0002	6.6	-	0.110	268	1.15	8.0	292
	14.3.70	1434	8.2	-	0.004	269	1.22	13.3	32
	14.3.70	1741	8.6	-	-0.006	269	1.46	10.3	20
	14.3.70	2008	7.7	-	0.003	270	1.39	9.2	9
	14.3.70	2221	6.2	-	0.029	269	1.34	8.4	359
	16.3.70	1829	6.0	-	0.019	269	1.67	10.0	120
	16.3.70	1916	9.6	-	0.002	270	1.32	14.4	111
	16.3.70	2302	16.4	-	0.000	269	1.22	35.5	70
	17.3.70	1959	9.9	-	0.002	270	1.66	29.0	317
	17.3.70	2130	8.4	-	0.016	270	1.57	25.6	314
	17.3.70	2344	5.4	-	0.033	270	1.32	20.4	310
	18.3.70	1520	7.3	-	-0.001	270	1.33	18.2	318
	23.3.70	1533	10.2	-	-0.015	266	1.61	12.5	114

*Site Location see Table 2.2

TABLE 2.3 (Cont'd)

Observed and Calculated Wind Field Parameters

Site No.*	Date	GMT	Observed U $m\ s^{-1}$	Observed θ_U Deg.	Observed z/L -	Observed T_a ^0K	Observed $10^3 C_d^a$ -	Calculated G $m\ s^{-1}$	Calculated θ_G Deg.
4a	30.3.71	2207	5.8	338	-0.130	251	1.64	7.7	19
	30.3.71	2330	6.6	338	-0.030	251	1.71	8.4	21
	1.4.71	0132	5.5	359	-0.180	249	1.57	7.5	16
	1.4.71	0239	4.4	3	0.000	245	1.62	8.1	13
	1.4.71	2045	9.2	227	0.150	250	1.79	13.7	321
	1.4.71	2202	9.8	227	0.100	251	1.54	13.6	320
	1.4.71	2309	9.9	225	0.380	250	0.95	13.5	320
	2.4.71	0123	10.1	228	0.340	248	1.10	12.0	313
	2.4.71	0629	8.4	235	-0.080	248	2.19	6.5	293
4b	5.4.71	2326	3.7	357	-0.100	243	1.03	4.7	66
	6.4.71	0057	4.3	14	0.100	243	1.16	4.9	63
	6.4.71	1717	5.7	12	-0.090	237	1.07	5.7	69
	6.4.71	1905	5.3	6	-0.110	237	1.13	6.2	66
	6.4.71	2048	5.8	1	-0.160	237	1.21	7.1	59
	6.4.71	2358	6.4	357	0.080	239	1.24	8.6	46
	7.4.71	0256	5.3	356	0.100	239	1.15	7.6	41

*Site Location see Table 2.2

TABLE 2.3 (Cont'd)

Observed and Calculated Wind Field Parameters

Site No.*	Date	GMT	Observed					Calculated	
			U $m\ s^{-1}$	θ_U Deg.	z/L -	T_a ^0K	$10^3 C_d^a$	G $m\ s^{-1}$	θ_G Deg.
5	30.3.72	2141	6.7	222	-0.012	245	1.94	12.7	297
	31.3.72	0536	6.4	268	0.048	246	1.52	10.0	298
	31.3.72	0712	6.4	267	0.044	247	1.56	9.1	299
	31.3.72	0836	6.8	270	0.044	247	1.61	8.9	301
	3.4.72	2029	6.6	85	-0.014	249	1.64	7.0	128
	3.4.72	2212	6.6	68	-0.017	253	1.94	6.3	120
	4.4.72	0122	6.3	66	-0.006	252	1.92	5.9	110
	4.4.72	0320	6.8	64	0.013	252	1.84	6.6	106
	4.4.72	0812	5.8	67	0.033	249	1.82	9.9	91
	4.4.72	0900	5.9	65	0.039	249	1.72	10.8	87
	4.4.72	2036	7.0	76	-0.023	251	2.00	5.4	79
	4.4.72	2307	5.1	67	-0.057	253	2.28	5.6	69
	10.4.72	0210	3.4	17	0.075	250	1.78	2.5	152
	12.4.72	0833	7.4	60	-0.056	249	1.65	8.6	115
	12.4.72	2027	9.8	61	-0.006	252	1.67	12.5	99
	12.4.72	2216	10.2	61	-0.007	253	1.60	12.0	98
	13.4.72	0122	11.0	64	0.002	254	1.89	11.7	97
	13.4.72	0722	10.2	58	0.014	254	2.04	12.0	97
	13.4.72	1952	10.1	55	0.001	254	2.10	14.7	92
	14.4.72	0036	9.5	59	0.000	255	2.38	15.9	87
	17.4.72	2231	7.6	83	-0.020	257	1.72	11.0	91
	18.4.72	0051	7.2	72	-0.015	257	1.98	12.6	91
	18.4.72	0137	7.3	79	-0.014	256	1.72	13.0	90
	18.4.72	0307	6.9	80	-0.050	254	1.41	13.9	89

*Site Location see Table 2.2

TABLE 2.3 (Cont'd)

Observed and Calculated Wind Field Parameters

Site No.*	DATE	GMT	Observed U $m\ s^{-1}$	Observed θ_U Deg.	Observed z/L -	Observed T_a $^{\circ}K$	Observed $10^3 C_d^a$ -	Calculated G $m\ s^{-1}$	Calculated θ_G Deg.
6	19.7.72	0024	5.9	235	0.000	274	2.61	5.5	279
	19.7.72	0213	9.1	218	0.010	275	2.02	7.7	273
	19.7.72	0408	8.4	224	0.021	274	2.52	10.0	265
	19.7.72	0526	9.7	233	0.029	276	1.87	11.6	260
	19.7.72	0653	14.6	197	0.010	276	2.30	13.9	257
	19.7.72	0748	13.7	188	0.016	276	2.16	15.5	256
	19.7.72	0853	12.3	185	0.010	276	1.94	17.5	256
	19.7.72	0933	14.1	190	0.010	276	2.38	18.7	255
	21.7.72	1359	8.9	218	0.018	276	2.01	5.4	284
	21.7.72	1658	10.0	198	0.030	276	1.56	7.2	273
	21.7.72	1744	6.1	207	0.051	276	1.75	7.6	271
	23.7.72	1355	9.6	226	0.013	276	2.35	10.1	279
	23.7.72	1448	3.3	227	0.138	276	2.08	8.7	276
	23.7.72	1557	9.7	215	0.016	276	1.91	6.9	272
	23.7.72	1655	10.5	221	0.012	276	1.96	5.4	269
	23.7.72	1905	9.8	219	0.004	277	2.40	7.9	264

*Site Location see Table 2.2

values of G_0 and θ_{G0} and related parameters (Appendix B1). Values of G_0 and θ_{G0} were adjusted by linear interpolation to the mean surface observation time of U and θ_U and were designated G and θ_G respectively. These data are presented in Table 2.3.

The correlation coefficient was calculated from the data at each site (Table 2.4). A significantly high correlation indicates that the geostrophic wind speed can be used to predict surface wind speed. The data for all sites (except Site No.1) are plotted in Appendix K and the linearity of the relationship at each site can be judged from these graphs.

TABLE 2.4

Correlations between Surface and Geostrophic Wind Speeds

Site No.	1	2	4a	4b	5	6
r	-0.58	0.63	0.78	0.84	0.68	0.68

The values of the correlation coefficients for these sites, with the exception of Site No. 1, indicate that a linear relationship exists between the observed and calculated values of the wind speeds (Li, 1964). The values of G for Site No. 1 calculated from surface weather charts are smaller than the corresponding observed values of U. On the other hand, Smith, Banke and Johannessen (1970) calculated larger values for G at the same site. A possible explanation for this discrepancy is that the isobars on the surface weather charts were too widely spaced, resulting in a negative correlation coefficient. Data for Site No. 1 were omitted in further analyses of the relationship between U and G. The actual sample, therefore, consists of 76 observations recorded at the five remaining sites.

TABLE 2.5

Correlations between
Surface and Geostrophic Wind Directions

Site No.	1	4a	4b	5	6
r	0.64	0.94	0.65	0.94	0.62

The high values of the correlation coefficients for these sites show that the surface wind direction can be determined from the geostrophic wind direction.

2.4 Estimating the Surface Wind Speed

Hasse's empirical equation can be written as

$$U_i = a_i G + b_i \qquad (2.3)$$

where U_i represents three estimates of U designated as U_1, U_2 and U_3. Differences among U_1, U_2 and U_3 result from variations of a_i and b_i, which may or may not vary with latitude or atmospheric stability (Hasse and Wagner, 1971; Hasse, 1974a, 1974b). These estimates were applied to the sites using the data from Table 2.3; this is graphically presented in Appendix K. For neutral stability with no dependence on latitude

$$U_1 = 0.54G + 1.68 \qquad (2.4)$$

For neutral stability with a dependence on latitude

$$U_2 = a_2 G + b_2 \qquad (2.5)$$

Values of a_2 and b_2 are represented in Table 2.6.

TABLE 2.6

Values of a_2 and b_2 for Use in Equation (2.5)
derived from Hasse and Wagner (1971) by Linear Interpolation

Site No.	2	4a	4b	5	6
Latitude (ϕ)	47°	74°	74°	75°	82°
a_2	0.519	0.628	0.628	0.630	0.640
b_2	2.59	2.05	2.05	2.05	2.00

For variable stability and no dependence on latitude

$$U_3 = a_3 G + b_3 \qquad (2.6)$$

in which

$$a_3 = 0.54 - 0.012\ \Delta T \qquad (2.6.1)$$

and

$$b_3 = 1.68 - 0.105\ \Delta T \qquad (2.6.2)$$

Values of a_3 and b_3 could have been calculated provided that ΔT, Hasse's atmospheric stability index, was applicable also to sea ice surfaces and that both T_a and T_{ice} were known for the sites. It may be assumed that ΔT is applicable to sea ice surfaces because values of atmospheric stability obtained over both sea and sea ice surfaces are similar (compare Roll, 1965 with Table 2.3 in this study). However, values of T_{ice} were not reported from the sites. ΔT was, therefore, calculated from the available stability parameter z/L^* (Table 2.3) where z is the height above the surface and L the Monin-Obukhov stability length (Banke and Smith, 1973). This was done by replacing z/L with the gradient form of the Richardson number Ri* (McIntosh and Thom, 1972).

$$Ri = (g/T_a)(dT/dz)/(dU/dz)^2 \qquad (2.7)$$

where g is the acceleration of gravity. Replacing the differentials with finite differences and using the values $\Delta z = z = 10m$, $\Delta U = U$ and $g = 9.81 ms^{-2}$

$$\Delta T = RiT_a\ U^2/98.1 \qquad (2.8)$$

---

*A parameter expressing stability conditions in the atmosphere in terms of a non-dimensional number: negative values indicate unstable conditions; nil values indicate neutral stability; positive values indicate stable conditions.

For unstable conditions Ri=z/L (Dyer and Hicks, 1970). Hence equation (2.8) becomes

$$\Delta T = (z/L)T_a U^2/98.1 \qquad (2.9)$$

For stable conditions Ri may be approximated by Ri=(z/L)/(1+5z/L) (Dyer, 1974), provided that $0.0<z/L<0.2$ (Munro, 1975). Hence, equation (2.8) becomes

$$\Delta T=(z/L)T_a U^2/98.1\ (1+5z/L) \qquad (2.10)$$

Values of U, G, U_1. U_2. U_3 and ΔT are presented in Appendix B2.

In order to select the most suitable version among equations (2.1), (2.4), (2.5) and (2.6) for estimating U from the values of G, U_1, U_2, U_3 they were compared with the observed values of U, using the χ^2 criteria* (defined in Table 2.7) which measures the discrepancies between each one of the calculated values of G, U_1, U_2, U_3 and the observed value of U at each site (Table 2.7). Here χ^2 should be referred to as a relative index only. Its value is directly related to the number of observations at a site and inversely related to the discrepancy between the calculated and the observed values of the wind speed. Consequently, the lowest value of χ^2 at a site provides the best estimate for U at that site.

An overall evaluation of the estimates required the

*The criterion is a weighted sum of squares, which give less weight to discrepancies in the higher range of U, where the prediction is

TABLE 2.7

Values of χ^2

Site No.	Lat. ^{0}N	No. of Observt'ns	$\chi^2=\Sigma\frac{(G-U)^2}{U}$	Rank	$\chi_1^2=\Sigma\frac{(U_1-U)^2}{U}$	Rank	$\chi_2^2=\Sigma\frac{(U_2-U)^2}{U}$	Rank	$\chi_3^2=\Sigma\frac{(U_3-U)^2}{U}$	Rank
2	47	20	170.3	4	30.4	2	31.1	3	26.7	1
4a	74	9	10.7	3	2.4	1	3.2	2	28.1	4
4b	74	7	2.6	4	0.3	1	1.4	2	1.8	3
5	75	24	42.0	4	6.7	1	11.6	3	8.5	2
6	82	16	19.2	2	19.7	3	14.3	1	28.8	4
Σ	-	76	-	17	-	8	-	11	-	14

elimination of the effect of the number of observations on χ^2. This was done by ranking the values of χ^2 at each site (1 for the lowest, 2 for the second lowest, 3 for the third lowest, 4 for the highest). These ranks as well as their sums for χ_0^2, χ_1^2, χ_2^2 and χ_3^2 are presented in Table 2.7. Since χ_1^2 has the lowest ranking, equation (2.4) provides the best estimate of U from G.

2.5 Minima and Maxima of the Mean Cross Isobar Angle

Means of the cross isobar angles $\overline{\Delta\theta}$ were estimated for each site using data from Table 2.3. They vary between 35^0 and 60^0. Values of the standard deviation of $\overline{\Delta\theta}$ (Table 2.8) are similar to those calculated by Hasse (1974b). $\overline{\Delta\theta}$ over sea surfaces (Table 2.1) varies between 2^0 and 35^0. As sea and sea ice surfaces have similar drag coefficients it may be assumed that $\overline{\Delta\theta}$ over sea ice varies

TABLE 2.8

Calculated Mean Values of $\Delta\theta$ over Sea Ice

Site No.	No. of Obser.	Mean $\Delta\theta$ Deg.	s.d. of $\Delta\theta$
1	5	59.2	7.1
4a	9	59.6	33.7
4b	7	55.3	8.2
5	24	35.4	27.4
6	16	55.5	12.8

between 0^0 and 60^0.

2.6 Conclusions

Surface weather charts are a reliable source for calculating speed and measuring direction of the geostrophic wind over sea ice; speed of the surface wind over sea ice may be estimated from the geostrophic wind by Hasse's equation $U = 0.54G + 1.68$, which is the best among three versions suggested by him; U_1 does not depend on latitude or stability; means of the cross isobar angle $\overline{\Delta\theta}$, over sea ice, vary between $0.^0$ and 60^0.

CHAPTER 3

GEOSTROPHIC WIND AND DRIFTING ICE VELOCITIES IN THE AREA DURING THE PERIOD OF STUDY

3.1 Measuring Sea Ice Velocity from LANDSAT Images

A number of techniques were previously used for calculating the velocity of drifting sea ice from sequential LANDSAT-1 MSS images. Crowder et al. (1973) were the first to measure sea ice motions from LANDSAT-1 images. They selected a sequence of four cloudless days and calculated the vorticity, divergence and velocity of the drifting pack ice using two strain arrays. The points which formed the two initial circular strain arrays were recognized on later images by refrozen fracture patterns. The same data and techniques were used by Hibler III et al. (1974) to study the motion of pack ice in the Arctic ocean. Wendler and Jayaweera (1974) measured the change in speed and direction of drifting ice floes between sequential paths by superimposing a positive transparency on a negative transparency of the next day. The measurements were obtained, after the composite transparencies were photographed, by detecting different grey tones on the prints. Nye and Thomas (1974) and Nye (1975) superimposed two positive transparencies of sequential orbital paths. They measured the motions by rotating the images relative to one another to obtain the best fit. The lack of agreement that remained was shown to be a measure of the strain. Sobczak (1977) determined speed and direction of ice movement from LANDSAT-1 images, using a plastic overlay on which ice features were drawn

for alternate days. Each overlay included an outline of the coast which provided the control points.

In this study, the velocities of drifting ice floes were calculated by measuring the co-ordinates of their centres on sequential LANDSAT-1 images, for which the mean scanning times were known. The procedure employed is presented in Sections 3.3 to 3.6. Values of these parameters as well as the geostrophic wind fields and air density are tabulated in Appendix J.

3.2 Geostrophic Wind Fields

Mean geostrophic wind fields for six cycles were obtained by the same techniques as those employed in Section 2.2. The measured and derived quantities p_1, T_{a_1}, ρ_{a_1}, Δn_1, G_1 and θ_{G_1} are grouped according to cycles in Appendix C. Data were rejected, however, if isobaric patterns were too complex to allow unambiguous measurements. ρ_{a_2}, G_2 and θ_{G_2} (Appendix C) were calculated from ρ_{a_1}, G_1 and θ_{G_1} respectively, by linear interpolation over 6 to 60 hours. Keels may extend as much as 10m below the subsurface of sea ice (Williams, Swithinbank and Robin, 1975) acting as a fixed rudder. Therefore an ice floe takes three to four hours to fully adjust its motion to a change in wind velocity (Fel'zenbaum, 1958) and interpolations over longer periods might be misleading. ρ_{a_3}, G_3 and θ_{G_3} (Appendix D) were adjusted from 0000, 0600, 1200 and 1800 GMT to t_i (the mean scanning time of a LANDSAT-1 MSS image) to t_i + 06:01'25"*, to t_i + 12:02'50" and to t_i + 18:04'15" by linear interpolation. ρ_{a_4}, G_4 and θ_{G_4} (Appendix J) are the means

*$(t_{i+1}-t_i)/4$ = 24:05'40"/4 = 06:01'25"

ρ_{a3}, G_3 and θ_{G_3} respectively. They were calculated for the intermediate scanning time $t_{1,i+1}$ ($t_{1,i+1} = t_i + 12{:}02'50''$) and provided the data source for calculating the motion of drifting groups of detached ice floes.

3.3 Selecting LANDSAT-1 Images for this Study

The selection involved locating three or preferably four sidelapping rows of sequential paths belonging to the same cycle, on which a group of ice floes was always recorded. The study area is covered by 36 frames during each cycle (3 rows of 12 paths). Each frame consists of 4 images, namely: MSS*-4 (500-600nm), MSS-5 (600-700nm), MSS-6 (700-800nm) and MSS-7 (800-1100nm). From the launch of LANDSAT-1 on 23 July, 1972 (Reeves, 1975) up to 30 July, 1976, 81 cycles had covered the study area. The theoretical number of images for this period and area is 2916 x 4 (NASA, 1976). The required images were selected from the ERTS (LANDSAT) Imagery Catalogue, updated to 19 March 1975 (CCRS, 1975) and computer lists, updated to 31 December, 1976 obtained from CCRS**. Even images having cloud coverage of up to 100% or images defined as being of poor quality (CCRS, 1975) were considered for selection.

An inspection of the lists showed that only sporadic coverage was available for 1972 (4 x 58 images) and 1976 (4 x 8 images). Therefore, images were selected from the years 1973 (4 x 251 images), 1974 (4 x 353 images), and 1975 (4 x 176 images).

---

* Multispectral Scanner
** Canada Centre for Remote Sensing

Images are tabulated in Appendix E according to cycle, row, path and date. An available image is represented by the percentage of cloud cover. All overlapping images belonging to three or four sequential paths were inspected. Italicized percentage of cloud cover denotes images that were selected for study. These images are listed in Table F1.

Prints, transparencies and enlargements (Table F2) of six selected cycles were used. Six images, one for each cycle, are presented in Appendix G (Figures G1.1-G6.1). Bare or snow covered sea ice, having high reflectance, stands out clearly against water surfaces, having high absorptance (Reeves, 1975). These differences are expressed in the sharp tonal differences recorded on MSS-4,5,6 and 7 images. However, where available, MSS-7 (800-1100nm) and MSS-5 (600-700nm) were used; the reasons were: tonal difference between water and ice are the strongest on MSS-7 images. Hence, detection of ice edges are best from these images. Variations in ice thickness may be evaluated by determining the stage of melting, e.g. shallow puddles (thicker ice) versus thaw holes (thinner ice). Shallow puddles are penetrated by radiation at the MSS-4 and MSS-5 wavelengths (McLain, 1972). MSS-5 was used rather than MSS-4 because of its better haze penetration. Simultaneous use of MSS-7 and MSS-5 images may, thus, help to qualitatively determine the relative thickness of sea ice.

3.4 Co-ordinates and Areas of Single Ice Floes

3.4.1 Co-ordinates of the single ice floe

Each ice floe belonging to a particular group is denoted by an identification number. This number is

retained for all paths in the same cycle (Appendix G). The criterion used for selecting individual ice floes was consistency of plan configuration in all the paths. Surface patterns were not required to arrive at a positive identification. A group can consist of any number of single ice floes in close proximity. The size of the group is determined by the availability of such floes. The number in each group varies from 3 to 26.

True north is indicated by the positive direction of the y axis in a cartesian co-ordinate system. A line was drawn on one image for each cycle, using two 1:1,000,000 maps* as references. The slight difference between the maps plotted in a Lambert Conformal Conic Projection and the images processed in a Space Oblique Mercator Projection can be neglected at this scale (Colvocresses, 1974; Kratky, 1974).

The origin was always located on land to secure positive and exact identification. Whenever possible it was located to the southwest of the group so that the ice floes would have positive x and y readings. Three to six control points common to side-lapping or overlapping images were marked on the prints. These points provided a means by which the planimetric relationships could be controlled.

The co-ordinates were read from 1:1,000,000 prints of the LANDSAT-1 images using a Ruscom Digitizer**. The co-ordinates denote the geometric centre of an ice floe or of a control point. The mean was calculated from three

---

* Firth River, NR-7/8/9, 1976 and Horton River, NR-9/10/11/12, 1976, compiled by the Survey and Mapping Branch, Ottawa, Canada.

** Model 21, Electronic Systems, Downsview, Ontario Canada.

independent readings. Deviations from the mean did not exceed $\pm$0.01" ($\pm$254m on the surface).

The x_i, y_i co-ordinates of each floe for each of the images are grouped in Appendix H according to cycles. The co-ordinates refer to the mean scanning time (t_i).

3.4.2 Area of the single ice floe

The mean area A_i of each ice floe was calculated from enlargements (Table F2) at a scale of about 1:250,000. Measurements were made by the dot-counting method. The value of A_i represents a mean of three independent counts. The results are grouped in Appendix H. The deviations from the mean value of A_i did not exceed $\pm 10^6 m^2$ for a single ice floe. The deviation from the mean area of a group ΣA_i ranges from $\pm$1.0% to $\pm$4.5%.

3.5 Co-ordinates of the Centre of Gravity of a Group

The co-ordinates of the centre of gravity of a group of ice floes X_{gr}, Y_{gr} were calculated from

$$X_{gr} = \Sigma A_i x_i / \Sigma A_i \qquad (3.1)$$

and

$$Y_{gr} = \Sigma A_i y_i / \Sigma A_i \qquad (3.2)$$

The results are grouped according to cycle in Appendix I and presented in Figures G1.2-G6.2. Reasons for calculating the co-ordinates for the centre of gravity rather than using the co-ordinates of single ice floes are:

a) the velocity of the centre of gravity of the group does not change if two or more ice floes belonging to the same group collide during the time interval between two paths

b) using co-ordinates of the centre of gravity reduces substantially the number of variables.

3.6 Mean Velocity of a Drifting Group

Assuming no acceleration (Section 1.3) the component mean velocities of the drifting centres of gravity, V_x, V_y, were calculated for the intermediate scanning time ($t_{i,i+1}$) from

$$V_x = \Delta X_{gr}/\Delta t \qquad (3.3)$$

and

$$V_y = \Delta Y_{gr}/\Delta t \qquad (3.4)$$

where Δt is the time increment between sequential paths and ΔX_{gr} or ΔY_{gr} are the component distance increments during Δt. The results (Appendix J) show that the geostrophic wind speed is greater than the ice speed by two orders of magnitude.

CHAPTER 4

PREDICTION OF ICE FLOE MOTIONS AND ASSOCIATED PARAMETERS

4.1 Minima and Maxima of Ice Thickness and Drag Coefficients

The key part of the method to predict the motions of wind driven groups of detached ice floes and for deriving the values of the parameters $\Delta\gamma$, $\Delta\theta$, h, C_d^a and C_d^w, associated with these motions is presented, tested and evaluated in this chapter. This was accomplished in six steps. First, minima and maxima of h, C_d^a and C_d^w were obtained from previous measurements. These are:

$$0.00 = h_{min} \leq h \leq h_{max} = 3.00 \text{ m}$$

$$0.95 = C_{d\ min}^a \leq 10^3 C_d^a \leq C_{d\ max}^a = 4.00$$

and

$$3.32 = C_{d\ min}^w \leq 10^3 C_d^w < C_{d\ max}^w = 57.17$$

The maximum thickness measured for the study area (AES, 1973, 1974, and 1975) is less than 3m but Pounder (1965) has suggested a range of 3-4m for the maximum thickness of old ice. Minimum and maximum values of C_d^a were determined from data summarized in Table 4.1 and from the work of Brown (1976). The range of values for C_d^w was determined from data summarized in Table 4.2.

TABLE 4.1

Drag Coefficients at the Air/Ice Interface: Summary of Published Results, (z=10m)

°N	°W	Date	No. of Obser.	Drag Coefficient Range 10^3 C_d^a	Drag Coefficient Mean 10^3 C_d^a	Stability Range z/L	Reference
–	–	7-57.9.58	186	–	1.44	Near Neutral	Untersteiner & Badgeley, 1965
48	64	13-20.2.69	9	2.20–4,00	3.09	-0.115–0.001	Smith, Banke & Johannesser, 1970
47	63	4-30.3.70	56	1.01–2.30	1.42	-0.081–0.110	Smith, 1972
47	63	7-14.3.70	74	1.60–2.40	1.70	-0.030–0.035*	Seifert & Langleben, 1972
47	63	19-27.3.70	181	1.80–3.20	2.20	-0.030–0.035*	Seifert & Langleben, 1972
71	131	30.6.70	3	2.27–2.87	2.57	0.039–0.095	Banke & Smith, 1971
74	131	30.3- 2.4.71	9	0.95–2.19	1.57	-0.180–0.380	Banke & Smith, 1973
74	131	5- 7.4.71	8	1.01–1.24	1.13	-0.160–0.100	Banke & Smith, 1973
70	133	20.4-11.5.71	46	1.66–1.69	1.68	Near Neutral	Langleben, 1972
70	133	20.4-11.5.71	92	1.95–2.46	2.28	Near Neutral	Langleben, 1972
75	150	30.3-18.4.72	30	1.11–2.38	1.82	-0.120–0.120	Banke & Smith, 1973
75	148	31.3-12.4.72	64	1.39–1.77	1.58	-0.040–0.050*	Langleben & Pounder, 1975
75	148	31.3-12.4.72	64	1.49–1.99	1.74	-0.040–0.050*	Langleben & Pounder, 1975
82	60	19-23.7.73	18	1.56–2.61	2.08	0.000–0.138	Banke & Smith, 1973
Summary of Results			840	0.95–4.00	–	-0.180–0.380	–

*Originally given in terms of Ri; Dyer's equation (Dyer,1974) was used to calculate the value of z/L.

TABLE 4.2

Drag Coefficients at the Water/Ice Interface: Summary of Published Results, (z=0.5m)

°N	°W	Date	No. of Obser.	Drag Coefficient Range $10^3 C_d^w$	Drag Coefficient Mean $10^3 C_d^w$	Thickness h m	Reference
75	14	Feb. & Mar.,1965	16	4.35-57.17	-	5.00	Untersteiner & Badgeley, 1965
-	-	1965	-	3.32- 7.60	5.46	-	Wu, 1972
48	64	-	-	20.00-47.00		-	Johannessen, 1970
90	-	1969	-	-	9.00	-	Johannessen, 1970
-	-	-	-	-	3.40	-	McPhee & Smith, 1975
Summary of Results			-	3.32-57.17	-	-	-

4.2 The Angle of Sea Ice Deflection

The angle of sea ice deflection was determined as follows. Resolving the x and y components of $\vec{t}_a$, $\vec{t}_w$ and $\vec{C}$, from equations (1.4), (1.5) and (1.6), allows equation (1.3) to be written as

$$\rho_a C_d^a U^2 \cos \Delta\gamma = \rho_w C_d^w V^2 \qquad (4.1)$$

and

$$\rho_a C_d^a U^2 \sin \Delta\gamma = \rho_{ice} f h V \qquad (4.2)$$

Eliminating V

$$\sin^2 \Delta\gamma / \cos \Delta\gamma = (\rho_{ice}^2 f^2 h^2 / \rho_a \rho_w C_d^a C_d^w)(1/U^2) \qquad (4.3)$$

Let

$$q = (\rho_{ice}^2 f^2 h^2 / \rho_a \rho_w C_d^a C_d^w)(1/U^2) \qquad (4.4)$$

Then

$$\sin^4 \Delta\gamma = q^2 - q^2 \sin^2 \Delta\gamma \qquad (4.5)$$

or

$$\sin^4 \Delta\gamma + q^2 \sin^2 \Delta\gamma - q^2 = 0 \qquad (4.6)$$

and

$$\sin \Delta\gamma = \{q[(q^2 + 4)^{0.5} - q]/2\}^{0.5} \qquad (4.7)$$

If $h \to 0$ then (equation 4.3) $\Delta\gamma_{min} \to 0$. The mean angle of sea ice deflection $\overline{\Delta\gamma}$ is

$$\overline{\Delta\gamma} = 0.5(\Delta\gamma_{max} + \Delta\gamma_{min}) = 0.5\Delta\gamma_{max} \qquad (4.8)$$

Values of $\Delta\gamma_{max}$ were calculated from equation (4.7), for intervals of 1 ms^{-1} of G*, using h_{max}, $C_{d\ min}^{a}$ and $C_{d\ min}^{w}$ assuming $\rho_w = 1.03\ 10^3 kg\ m^{-3}$, $\rho_{ice} = 0.91\ 10^3 kg\ m^{-3}$ and a mean latitude of 70^0. The values of $\Delta\gamma_{max}$ are presented in Table 4.3.

4.3 Values of the Cross Isobar Angle

The cross isobar angle may be obtained from the difference between equations (1.8) and (1.7) written as

$$\Delta\theta = \Delta\gamma + \theta_G - \theta_{ice} \qquad (4.9)$$

---

*$\Delta\gamma_{max}$ was estimated for G rather than for U to leave room for further refinements in the values of a and b in Hasse's equation (2.4).

TABLE 4.3

Maximum Angle of Ice Deflection ($\Delta\gamma_{max}$) for Intervals of 1 m s^{-1} of the Geostrophic Wind Speed (G)

G m s^{-1}	$\Delta\gamma_{max}$ Deg.	G m s^{-1}	$\Delta\gamma_{max}$ Deg.	G m s^{-1}	$\Delta\gamma_{max}$ Deg.
1.00	82.25	18.00	29.38	35.00	16.56
2.00	78.26	19.00	28.12	36.00	16.14
3.00	73.76	20.00	26.95	37.00	15.75
4.00	69.02	21.00	25.88	38.00	15.37
5.00	64.29	22.00	24.89	39.00	15.01
6.00	59.77	23.00	23.97	40.00	14.66
7.00	55.59	24.00	23.11	41.00	14.34
8.00	51.77	25.00	22.31	42.00	14.02
9.00	48.33	26.00	21.57	43.00	13.72
10.00	45.24	27.00	20.87	44.00	13.43
11.00	42.48	28.00	20.21	45.00	13.15
12.00	39.99	29.00	19.60	46.00	12.89
13.00	37.76	30.00	19.02	47.00	12.63
14.00	35.75	31.00	18.47	48.00	12.39
15.00	33.92	32.00	17.95	49.00	12.15
16.00	32.27	33.00	17.46	50.00	11.93
17.00	30.76	34.00	17.00		

Values of the minimum, maximum and mean of $\Delta\theta$ were calculated (Tables 4.4.1 and 4.4.2) from this equation, using $\Delta\gamma_{min}=0$ (Section 4.2) and $\Delta\gamma_{max}$ (Table 4.3) respectively and θ_G and θ_{ice} (Appendix J). Values of $\overline{\Delta\theta}_4^*$, less than 0^0 or greater than 60^0, were not used for further calculation (Section 2.6). Cycles 21 and 60 and part of cycles 26b and 41 were, therefore, rejected. Table 4.5 shows a close relationship between the availability of measured values of θ_{g_1} and the acceptability of $\overline{\Delta\theta}_4$, with cycle 21 being the only exception.

4.4 Ratios between Sea Ice Thickness and Drag Coefficients

To determine the ratios between sea ice thickness and the drag coefficients, M and N were defined from equations (4.1) and (4.2) as

$$M = h/C_d^a = (\rho_a U^2 \sin\Delta\gamma)/(\rho_{ice} f V) \qquad (4.10)$$

and

$$N = C_d^w/C_d^a = (\rho_a U^2 \cos\Delta\gamma)/(\rho_w V^2) \qquad (4.11)$$

Then,

*The subscript $_4$ denotes quantities adjusted to LANDSAT-1 intermediate scanning time.

TABLE 4.4.1

Range of the Cross Isobar Angle $\Delta\theta_4$

Cycle No.	t_{12}			t_{23}			t_{34}		
	$\overline{G}_4$ m s^{-1}	$\Delta\theta_4$ Deg. min.	max.	$\overline{G}_4$ m s^{-1}	$\Delta\theta_4$ Deg. min.	max.	$\overline{G}_4$ m s^{-1}	$\Delta\theta_4$ Deg. min.	max.
21	12.0	-56	-16	7,3	-89	- 35	-	-	-
26a	5.5	2	64	8.4	- 8	42	7.7	- 20	32
26b	6.0	- 2	58	7.0	16	72	4.7	111	177
41	9.0	26	74	7.5	70	123	5.5	- 39	23
43	9.3	-10	37	9.3	-17	30	-	-	-
60	8.4	-98	-48	10.6	-49	- 5	-	-	-

TABLE 4.4.2

Range and Mean of the Cross Isobar Angle $\Delta\theta_4$

Cycle No.	t_{12} & t_{23}			t_{23} & t_{34}			t_{12} & t_{34}			t_{12}, t_{23} & t_{34}		
	$\Delta\theta_4$ Deg.			$\Delta\theta_4$ Deg.			$\Delta\theta_4$ Deg.			$\Delta\theta_4$ Deg.		
	min.	max.	mean	min.	max.	mean	min.	max.	mean	min.	max.	mean
21	*	*	*	-	-	-	-	-	-	-	-	-
26a	2	42	22	0	32	16	2	32	17	2	32	17
26b	16	58	37	*	*	*	*	*	*	*	*	*
41	70	74	72	*	*	*	*	*	*	*	*	*
43	0	30	15	-	-	-	-	-	-	-	-	-
60	*	*	*	-	-	-	-	-	-	-	-	-

* where $\overline{\Delta\theta_4} < 0°$ or $\overline{\Delta\theta_4} > 60°$

TABLE 4.5

Relationship between Availability of θ_{G_1} and Acceptability of $\Delta\theta_4$

			Availability of measured valued of θ_{G_1}			Acceptability of $\Delta\theta_4$	
Cycle	Mon.	Year	nearly always	partially	nearly never	acceptable	unacceptable
21	July	73	24/25-25/26	-	-	-	t_{12}, t_{23} -
26a	Oct.	73	23/24-25/26	-	-	t_{12}, t_{23}, t_{34}	-
26b	Oct.	73	25/26	26/27	27/28	t_{12}, t_{23} -	- t_{34}
41	July	74	-	-	24/25-26/27	t_{12} -	- t_{23}, t_{34}
43	Aug.	74	24/25-25/26	-	-	t_{12}, t_{23} -	-
60	June	75	-	24/25-25/26	-	-	t_{12}, t_{23} -

$$B = M/N = h/C_d^w \qquad (4.12)$$

The minima and maxima of B, M and N, determined from the minima and maxima of h, C_d^a and C_d^w, are

$$0.00 \leq B \leq 903.61 \text{ m}$$

$$0.00 \leq M \leq 3157.89 \text{ m}$$

and

$$0.83 \leq N \leq 60.18$$

Values of M and N, in the study area, were calculated for the intermediate scanning time, $t_{1\,1\,i+1}$*, by replacing $\Delta\gamma$, the parameters and the constants in equations (4.9), (4.10) and (4.11) with values from Appendix J and Section 4.2. The means $\bar{M}$ and $\bar{N}$ were calculated from the values of M and N for t_{12} & t_{23}, t_{23} & t_{34}, t_{12} & t_{34} and t_{12} & t_{23} & t_{34}. The mean B was calculated by replacing M and N in equation (4.12) with values of $\bar{M}$ and $\bar{N}$ for the same periods. The values of $\bar{B}$, $\bar{M}$ and $\bar{N}$, for the study area, are presented in Table 4.6.

---

*$t_{1\,1\,i+1} = t_{12}, t_{23}, t_{34} \ldots$

TABLE 4.6

Means of the Ratios B, M and N

Cycle No.	t_{12} & t_{23}			t_{23} & t_{34}		
	$\overline{B}$	$\overline{M}$	$\overline{N}$	$\overline{B}$	$\overline{M}$	$\overline{N}$
	m	m	-	m	m	-
26a	886.64	638.38	** 0.72	**970.94	980.65	1.01
26b	262.46	1225.71	4.67	*	*	*
41	156.09	543.19	3.48	*	*	*
43	127.10	**7945.24	**62.51	*	*	*

* Where $\overline{\Delta\theta_4} < 0^0$ or $\overline{\Delta\theta_4} > 60^0$

** Where the value of $\overline{B}$, $\overline{M}$ or $\overline{N}$ is either less than the corresponding minimum or greater than the corresponding maximum of B, M or N

TABLE 4.6 (Cont'd)

Means of the Ratios B, M and N

Cycle No.	t_{12} & t_{34}			t_{12}, t_{23} & t_{34}		
	$\overline{B}$	$\overline{M}$	$\overline{N}$	$\overline{B}$	$\overline{M}$	$\overline{N}$
	m	m	-	m	m	-
26a	837.14	795.28	0.95	864.02	777.62	0.90
26b	*	*	*	*	*	*
41	*	*	*	*	*	*
43	-	-	-	-	-	-

* Where $\overline{\Delta\theta_4} < 0^0$ or $\overline{\Delta\theta_4} > 60^0$

4.5 Ice Thickness and Drag Coefficients

To estimate the thickness and the drag coefficients for the area, during the period of study, equations (4.12) and (4.10) were rewritten, B and M were replaced by $\bar{B}$ and $\bar{M}$ (Section 4.4) and h was written for the minimum values of h, C_d^a and C_d^w (Section 4.1) as

$$h = C_d^w \bar{B} \geq 3.32\ 10^{-3}\ \bar{B}m \qquad (4.13)$$

$$h = C_d^a \bar{M} \geq 0.95\ 10^{-3}\ \bar{M}m \qquad (4.14)$$

$$h \geq 0.00\ m \qquad (4.15)$$

so that

$$h \geq \max.\{3.32\ 10^{-3}\bar{B},\ 0.95\ 10^{-3}\bar{M},\ 0.00\} = h_{LL} \qquad (4.16)$$

where h_{LL}, the lower limit of h, is the maximum (max.) value among the three values of h in equation (4.16). In the same way, h was written for the maximum values of h, C_d^a and C_d^w as

$$h \leq \min.\{57.17\ 10^{-3}\bar{B},\ 4.00\ 10^{-3}\bar{M},\ 3.00\} = h_{UL} \qquad (4.17)$$

where h_{UL}, the upper limit of h, is the minimum (min.) value among the three values of h in equation (4.17). Values of h are acceptable only between the limits

$$h_{LL} \leq h \leq h_{UL} \tag{4.18}$$

Value of C_d^a and C_d^w are acceptable only between the limits

$$h_{LL}/\bar{M} \leq C_d^a \leq h_{UL}/\bar{M} \tag{4.19}$$

and

$$h_{LL}/\bar{B} \leq C_d^w \leq h_{UL}/\bar{B} \tag{4.20}$$

Ranges of the values of h, C_d^a and C_d^w were calculated, for the study area, from equations (4.18), (4.19) and (4.20). Data on thickness measured at the nearest coastal stations, Tuktoyaktuk, Cape Perry and Sachs Harbour, N.W.T. (Figure 1.1), were obtained from published data (AES, 1974). Ranges of the values for these parameters are presented in Table 4.7.

If the calculated values of $\bar{B}$, $\bar{M}$ and $\bar{N}$ (Table 4.6) were either less than the corresponding minima, or greater than the corresponding maxima of B, M and N (Section 4.4) then the values of the lower limits of h, C_d^a and C_d^w were always greater than the upper limits of these parameters.

TABLE 4.7

Ranges of Ice Thickness and of the Drag Coefficients C_d^a and C_d^w
(Data on h, measured at coastal stations, is enclosed in parenthesis)

Cycle No.	for t_{12} & t_{23}			for t_{23} & t_{34}		
	h m	10^3 C_d^a -	10^3 C_d^w -	h m	10^3 C_d^a -	10^3 C_d^w -
26a	**2.93-2.55 (0.30-0.35)	**4.58-4.00	**3.32- 2.90	**3.23-3.00 (0.30-0.35)	**3.30-3.06	**3.32-3.08
26b	1.16-3.00 (0.30-0.35)	0.95-2.45	4.44-11.44	*	*	*
41	0.52-2.17 (1.07-1.80)	0.95-4.00	3.32-13.93	*	*	*
43	**7.55-3.00 (-)	**0.95-0.38	**59.39-23.60	-	-	-

* where $\overline{\Delta\theta}_4$ 0° or $\overline{\Delta\theta}_4 > 60^\circ$ (Table 4.5)

** where the value of $\overline{B}$, $\overline{M}$ or $\overline{N}$ is either less than the corresponding minimum or greater than the corresponding maximum of B, M or N.

TABLE 4.7 (Cont'd)

Ranges of Ice Thickness and of the Drag Coefficients C_d^a and C_d^w
(Data on h, measured at coastal stations, is enclosed in parenthesis)

Cycle No.	for t_{12} & t_{34}			for t_{12}, t_{23} & t_{34}		
	h m	10^3 C_d^a -	10^3 C_d^w -	h m	10^3 C_d^a -	10^3 C_d^w -
26a	2.78-3.00 (0.30-0.35)	3.49-3.77	3.32-3.59	2.87-3.00 (0.30-0.35)	3.69-3.86	3.32-3.47
26b	*	*	*	*	*	*
41	*	*	*	*	*	*
43	-	-	-	-	-	-

* where $\overline{\Delta\theta}_4 < 0^0$ or $\overline{\Delta\theta}_4 > 60^0$ (Table 4.5)

The results for cycle 43 (Table 4.7) were, therefore, unacceptable as estimates for h, C_d^a and C_d^w. The best results were obtained for cycles 26b and 41, where the values of $\bar{B}$, $\bar{M}$ and $\bar{N}$ (Table 4.6) were either greater than the minima or less than the maxima of B, M and N (Section 4.4). For the same reasons the results for cycle 26a were partially acceptable: The values for t_{12} & t_{23} and t_{23} & t_{34} were unacceptable and those for t_{12} & t_{34} and t_{12} & t_{23} & t_{34} were acceptable.

The calculated values of the ranges of h obtained for cycles 26a and 26b do not agree with those measured at the nearest coastal stations (Table 4.7). Freeze up along the west coast of the Mackenzie bay occurred on October 8, 1973 (LANDSAT-1 MSS 5 1442-20295, 72-11-25) and at Tuktoyaktuk, N.W.T. on October 9, 1973 (AES, 1974). Since only 0.25 - 0.50 m of ice could be formed during a period of 2-3 weeks (Pounder, 1965) it is suggested that values of h, measured during cycles 26a and 26b, provide a better approximation to the actual values than the calculated one. The calculated values of h_{LL} for cycle 26b is less than h_{LL} for cycle 26a and provides therefore, a better estimate for the actual value of h. The calculated values of h for cycle 41 were within the range of values measured at Sachs Harbour, N.W.T. (1.80 m) on June 14, 1974 and at Cape Parry, N.W.T. (1.07m) on July 5, 1974 (AES, 1974).

4.6 Predicting the Motions of Groups of Detached Ice Floes

The speed of motion for a drifting group of detached ice floes was predicted as follows. From equations (4.10) and (4.11)

$$D = \sin\Delta\gamma/V = (M\ \rho_{ice}\ f)/(\rho_a\ U^2) \qquad (4.21)$$

and

$$E = \cos\Delta\gamma/V^2 = (N\ \rho_w)/(\rho_a\ U^2) \qquad (4.22)$$

Adding the squares of these equations

$$\cos^2\Delta\gamma + \sin^2\Delta\gamma = (E\ V^2)^2 + (D\ V)^2 \qquad (4.23)$$

or

$$E^2V^4 + D^2V^2 - 1 = 0 \qquad (4.24)$$

Therefore

$$V = \{[(D^4 + 4E^2)^{0.5} - D^2]/2E^2\}^{0.5} \qquad (4.25)$$

Values of the speed of motion were then calculated for the cycles. D and E were determined using values of $\bar{M}$ and $\bar{N}$ (Table 4.6), ρ_a, (Appendix J), the surface wind speed, estimated from equation (2.4) and the values of G_a (Appendix J).

The direction of motion, for a drifting group of detached ice floes, was obtained by rewriting equation (4.9) as

$$\theta_{ice} = \Delta\gamma - \Delta\theta + \theta_G \qquad (4.26)$$

where $\Delta\gamma$ was calculated from equation (4.21) as

$$\sin \Delta\gamma = DV \qquad (4.27)$$

$\Delta\theta$ was replaced by the values of $\overline{\Delta\theta}_4$ from Table 4.4.2, assuming that $\overline{\Delta\theta}_4$ remains constant for the period between sequential orbital paths of LANDSAT-1 (24:05'40"). θ_G was replaced by the values of θ_{G4} from Appendix J. The velocities of motion predicted for the cycles are presented in Tables 4.8 - 4.11.

Velocities of the centres of gravity predicted for $t_{2,3}$ (Table 4.8) and for $t_{3,4}$ (Table 4.9 and Table 4.10) are comparable to those recorded on LANDSAT-1 MSS images. The calculated values of V and θ_{ice} at $t_{2,3}$ (Table 4.8) provide a close approximation to those observed on the images (Figures G1.2 and G2.2). The predicted value of V for $t_{3,4}$ (Table 4.9) is virtually identical to the corresponding observed values, but there is substantial difference between observed and calculated values of θ_{ice}. This is explained by the presence of a newly formed polynya* (Figures G3.1 and G3.2), which forced the group to float along its edge. A similar explanation is suggested for the disagreement

* Any non-linear shaped opening enclosed in ice.

TABLE 4.8

Cycle No. 26a

Measured Vs. Predicted Velocity of Centre of Gravity of Group of Detached Ice Floes

Velocity of Drifting Ice	Measured from LANDSAT-1 Imagery	Predicted from ρ_{a4}, G_4, θ_{G4}, V, θ_{ice} at				and from ρ_{a4}, G_4, θ_{G4} at
		t_{12} & t_{23}	t_{23} & t_{34}	t_{12} & t_{34}	t_{12}, t_{23} & t_{34}	$t_{1}i+1$ for
V 10^{-2} m s^{-1}	19.6	-	** 14.8	-	-	t_{12}
θ_{ice} Deg.	134	-	**159	-	-	
V 10^{-2} m s^{-1}	23.6	-	-	29.5	-	t_{23}
θ_{ice} Deg.	156	-	-	166	-	
V 10^{-2} m s^{-1}	16.9	** 37.3	-	-	-	t_{34}
θ_{ice} Deg.	179	**178	-	-	-	
V 10^{-2} m s^{-1}	-	** 32.9	** 24.1	27.6	28.3	t_{45}
θ_{ice} Deg.	-	**197	**214	206	206	
V 10^{-2} m s^{-1}	-	** 24.5	** 16.8	20.1	20.6	t_{56}
θ_{ice} Deg.	-	**231	**246	239	240	

** where the value of $\bar{B}$, $\bar{M}$ or $\bar{N}$ is either less than the corresponding minimum or greater than the corresponding maximum of B, M or N.

TABLE 4.9

Cycle No. 26b

Measured Vs. Predicted Velocity of Centre of Gravity of Group of Detached Ice Floes

Velocity of Drifting Ice	Measured from LANDSAT-1 Imagery	Predicted from ρ_{a4}, G_4, θ_{G4}, V, θ_{ice} at				and from ρ_{a4}, G_4, θ_{G4} at
		t_{12} & t_{23}	t_{23} & t_{34}	t_{12} & t_{34}	t_{12}, t_{23} & t_{34}	t_{11i+1} for
V 10^{-2} m s^{-1}	23.8	-	*	-	-	t_{12}
θ_{ice} Deg.	209	-	*	-	-	
V 10^{-2} m s^{-1}	6.3	-	-	*	-	t_{23}
θ_{ice} Deg.	269	-	-	*	-	
V 10^{-2} m s^{-1}	10.6	10.3	-	-	-	t_{34}
θ_{ice} Deg.	162	279	-	-	-	
V 10^{-2} m s^{-1}	-	13.6	*	*	*	t_{45}
θ_{ice} Deg.	-	289	*	*	*	

* where $\overline{\Delta\theta}_4 < 0^0$ or $\overline{\Delta\theta}_4 > 60^0$

TABLE 4.10

Cycle No. 41

Measured Vs. Predicted Velocity of Centre of Gravity of Group of Detached Ice Floes

Velocity of Drifting Ice	Measured from LANDSAT-1 Imagery	Predicted from ρ_{a4}, G_4, θ_{G4}, V, θ_{ice} at t_{12} & t_{23}	t_{23} & t_{34}	t_{12} & t_{34}	t_{12}, t_{23} & t_{34}	and from ρ_{a4}, G_4, θ_{G4} at t_{1i+1} for
V 10^{-2} m s^{-1}	34.0	-	*	-	-	t_{12}
θ_{ice} Deg.	104	-	*	-	-	
V 10^{-2} m s^{-1}	7.8	-	-	*	-	t_{23}
θ_{ice} Deg.	94	-	-	*	-	
V 10^{-2} m s^{-1}	5.1	14.6	-	-	-	t_{34}
θ_{ice} Deg.	238	148	-	-	-	
V 10^{-2} m s^{-1}	-	20.5	*	*	*	t_{45}
θ_{ice} Deg.	-	167	*	*	*	

*where $\overline{\Delta\theta_4} < 0^\circ$ or $\overline{\Delta\theta_4} > 60^\circ$

Table 4.11

Cycle No. 43

Measured and Predicted Velocity of Centre of Gravity of Group of Detached Ice Floes

Velocity of Drifting Ice	Measured from LANDSAT-1 Imagery	Predicted from ρ_{a_4}, G_4, θ_{G_4}, V, θ_{ice} at				and from ρ_{a_4}, G_4, θ_{G_4} at
		t_{12} & t_{23}	t_{23} & t_{34}	t_{12} & t_{34}	t_{12}, t_{23} & t_{34}	t_{1i+1} for
V 10^{-2} m s^{-1}	3.4	-	-	-	-	t_{12}
θ_{ice} Deg.	165	-	-	-	-	
V 10^{-2} m s^{-1}	2.4	-	-	-	-	t_{23}
θ_{ice} Deg.	164	-	-	-	-	
V 10^{-2} m s^{-1}	-	** 4.6	-	-	-	t_{34}
θ_{ice} Deg.	-	**178	-	-	-	

** where the value of $\overline{B}$, $\overline{M}$ or $\overline{N}$ is either less than the corresponding minimum or greater than the corresponding maximum of B, M or N

between the predicted and observed values of V and θ_{ice} at t_{34} (Table 4.10). After a day of relatively undisturbed motion inside a polynya, the group was trapped in an ice congested inlet (Figures G4.1 and G4.2). This, together with the rotational motions of individual floes as recorded on the LANDSAT-1 MSS images (Appendix F), can fully account for the deviation between observed and predicted motions. Results for t_{12} are presented in Table 4.8 to demonstrate that predicted values of V and θ_{ice} do not agree with the observed ones where the value of $\bar{B}$, $\bar{M}$ or $\bar{N}$ is either less than the corresponding minima or greater than the corresponding maxima of B, M or N. The other predicted values of V and θ_{ice} (Tables 4.8 - 4.11) could not be evaluated as simultaneous observations were not available.

CHAPTER 5

CONCLUSION

This study sought to develop a method for predicting the motions of wind-driven detached ice floes and for deriving the wind fields and sea ice parameters associated with their motions from sequential surface weather charts and remotely sensed data. To this end, the theory involved and the procedures developed were presented. The results were tested and evaluated. Five conclusions are reached.

a) Surface weather charts and LANDSAT-1 MSS images are the most suitable data sources for developing and testing the method; surface weather charts, because they are the only readily available data source for the geostrophic wind fields and associated data in the Arctic. MSS images have the advantage over images from other satellites of cartographic reliability and excellent resolution, which are essential for obtaining the best possible data from measurements of position and area of an ice floe. An examination of the next best images currently available, the NOAA-5* images, which are recorded during day and night with a cycle frequency of two overpasses per day, showed greater distortion and a ground resolution lower by more than one order of magnitude.

b) During the period 1972-1976, 2916 x 4 LANDSAT-1 MSS were recorded over the area of study. From these 846 x 4 images were processed by CCRS. They were all considered for possible application in this study. Only six cycles recorded on 18 x 2 images were found suitable for analysis. These images had been recorded infrequently because sequences of three or four cloud free days rarely coincided with the

* National Oceanographic and Atmospheric Administration, Satellite No. 5.

eighteen day cycles of LANDSAT-1. Thus, visible and reflected infrared sensor systems are of limited value for routine detection of sea ice motions.

c) For operational use it is recommended that the MSS data should be replaced by data from a microwave system, which is independent of sun illumination and cloud conditions. At the current state of the technology, radar systems are the best for this purpose, since they are able to provide the best available cartographic reliability and ground resolution. The operational airborne system, recently introduced to detect sea ice in the Canadian Arctic, is able to provide the data required for the method. The most advanced spaceborne radar systems are the experimental SEASAT-1* and the planned Canadian SURSAT**. This indicates that after the spaceborne systems planned for the next decade have become operational, the method may be applied on a global scale.

d) Information related to predictions, surface wind fields and ice thickness can be used to assist marine traffic and support exploration of natural resources. These data may be applied around the edges of the Arctic and Antarctic close pack ice, in polynyas, gulfs, straits and lakes.

e) Five parameters, essential to any study of the dynamics of open pack ice, which were formerly practically unavailable, may now be derived from the method. These are speed and direction of the surface wind over sea ice; thickness of the detached ice floes; drag coefficient at the air/ice interface and drag coefficient at the water/ice interface.

---

* SEA SATellite.

** SURveillance SATellite.

APPENDIX A

NOTATION

Upper Case Roman

A_i	area of a single ice floe	m^2
B	ratio between sea ice thickness and subsurface drag coefficient	m
C	horizontal Coriolis deflecting force per unit area of ice	$kg\ m^{-1}s^{-2}$
C_d^a	drag coefficient at the air/ice interface	dimensionless
G	horizontal geostrophic wind speed	$m\ s^{-1}$
I	internal ice stress	$kg\ m^{-1}s^{-2}$
L	Monin-Obukhov stability length	m
M	ratio between sea ice thickness and surface drag coefficient	m
N	ratio between surface and subsurface drag coefficients	dimensionless
P	horizontal marine pressure gradient stress	$kg\ m^{-1}s^{-2}$
R_d	gas constant for dry air	$J\ kg\ ^0K$
R_i	Richardson number	dimensionless

T_a	air temperature	^0K
T_{ice}	sea ice surface temperature	^0K
T_w	sea surface temperature	^0K
U	horizontal surface wind speed at 10m above the ice surface	$m\ s^{-1}$
U_i	estimates of U	$m\ s^{-1}$
V	speed of the centre of gravity of a drifting group of ice floes	$m\ s^{-1}$
V_x, V_y	component velocities of a drifting centre of gravity	$m\ s^{-1}$
X_{gr}, Y_{gr}	co-ordinates of the centre of gravity of a group of ice floes	m

Lower Case Roman

f	Coriolis parameter	s^{-1}
g	acceleration of gravity	$m\ s^{-2}$
h	ice thickness	m
n	horizontal distance measured normal to the isobars	m
p	atmospheric pressure	kPa
t	time	

t_i	mean scanning time of LANDSAT-1 image	Date HHMMSS
$t_{i,i+1}$	intermediate scanning time of LANDSAT-1 image	Date HHMMSS
x_i, y_i	co-ordinates of the geometric centre of a single ice floe	m
z	height above the surface	m
z/L	stability parameter	dimensionless

Upper Case Greek

ΔT	air-ice temperature difference	degree
ΔX_{gr}, ΔY_{gr}	component distance increments of a drifting centre of gravity between sequential paths of LANDSAT-1.	m
Δt	time increment between sequential paths of LANDSAT-1	s
$\Delta\gamma$	angle of sea ice deflection	degree
$\Delta\theta$	cross isobar angle	degree
ΣA_I	area of a group of ice floes	m^2

Lower Case Greek

θ_G	geostrophic wind direction	degree
θ_{ice}	ice motion direction	degree

θ_U	surface wind direction	degree
ρ_a	air density	kg m^{-3}
ρ_{ice}	sea ice density	kg m^{-3}
ρ_w	ocean water density	kg m^{-3}
τ_a	horizontal air stress at the air/ice interface	kg $m^{-1} s^{-2}$
τ_w	horizontal water stress at the water/ice interface	kg $m^{-1} m^{-2}$
ϕ	latitude	degree
ω	Earth's angular speed	s^{-1}

APPENDIX B1

GEOSTROPHIC WIND FIELDS AND RELATED PARAMETERS

p	atmospheric pressure
T_a	air temperature
ρ_a	air density
n	horizontal distance measured normal to the isobars
Δ	denotes finite differences of a quantity
G	geostrophic wind speed
θ_G	geostrophic wind direction
$_0$	denotes quantities with no time adjustments

TABLE B1.1

SITE NOS. 1 AND 2

Site No.*	Date	GMT	p kPa	T_a ^0K	ρ_a kg m^{-3}	Λ_n 10^3m	G_0 m s^{-1}	θ_{G_0} Deg.
1	20.2.69	1200	102.67	272	1.315	283.5	9.9	77
	20.2.69	1800	102.91	276	1.299	485.0	5.9	68
	21.2.69	0000	103.24	274	1.313	388.0	7.2	80
2	6.3.70	1800	100.92	271	1.298	375.5	7.7	30
	7.3.70	0000	100.75	271	1.295	319.0	9.1	18
	10.3.70	1200	99.54	264	1.314	250.3	11.4	273
	10.3.70	1800	98.59	265	1.296	483.4	6.0	286
	11.3.70	1800	99.18	267	1.294	404.9	7.2	258
	12.3.70	0000	99.40	267	1.297	225.8	12.8	292
	12.3.70	1200	99.99	269	1.295	157.1	18.4	282
	12.3.70	1800	100.01	268	1.300	274.9	10.5	290
	13.3.70	0000	100.41	271	1.291	277.3	10.5	292
	14.3.70	1200	99.65	270	1.286	184.1	15.8	41
	14.3.70	1800	99.70	270	1.287	292.0	10.0	19
	15.3.70	0000	99.98	271	1.285	373.0	7.8	351
	16.3.70	1800	101.20	270	1.306	395.1	7.3	125
	17.3.70	0000	99.80	270	1.288	71.2	40.9	60
	17.3.70	1800	100.56	270	1.298	85.9	33.6	320
	18.3.70	0000	101.19	270	1.306	144.8	19.8	310
	18.3.70	1200	101.90	270	1.315	127.6	22.4	317
	18.3.70	1800	102.00	273	1.302	193.9	14.9	318
	23.3.70	1200	102.03	269	1.322	363.2	7.8	96
	23.3.70	1800	101.54	270	1.310	182.8	15.7	126

*Site Location see Table 2.2

TABLE B1.2

SITE NOS. 4a AND 4b

Site No.*	Date	GMT	p kPa	T_a ^0K	ρ_a kg m^{-3}	Δn $10^3 m$	G_0 m s^{-1}	θ_{G_0} Deg.
4a	30.3.71	1800	101.28	243	1.452	345.5	5.7	13
	31.3.71	0000	101.45	244	1.449	228.5	8.6	22
	1.4.71	0000	103.11	241	1.491	289.5	6.6	25
	1.4.71	0600	103.47	237	1.521	186.7	10.0	7
	1.4.71	1800	103.33	242	1.488	139.3	13.8	323
	2.4.71	0000	102.89	246	1.457	144.9	13.5	319
	2.4.71	0600	102.48	241	1.482	267.5	7.2	293
	2.4.71	1200	102.53	241	1.482	312.1	6.2	292
4b	5.4.71	1800	102.58	245	1.459	596.2	3.3	81
	6.4.71	0000	102.63	249	1.436	409.6	4.9	14
	6.4.71	0600	102.48	244	1.463	381.7	5.1	54
	6.4.71	1200	102.54	243	1.470	353.8	5.5	59
	6.4.71	1800	102.41	243	1.468	339.9	5.7	6
	7.4.71	0000	102.65	242	1.478	225.7	8.6	46
	7.4.71	0600	102.62	240	1.490	289.8	6.6	35

*Site Location see Table 2.2

TABLE B1.3

SITE NO. 5

Site No.*	Date	GMT	p kPa	T_a ^0K	ρ_a kg m^{-3}	Δn $10^3 m$	G_0 m s^{-1}	θ_{G_0} Deg.
5	30.3.72	1800	102.55	244	1.464	197.8	9.8	298
	31.3.72	0000	102.67	246	1.454	133.7	14.6	297
	31.3.72	0600	102.95	243	1.476	197.8	9.7	298
	31.3.72	1200	102.74	243	1.473	245.2	7.9	304
	3.4.72	1800	101.31	248	1.423	250.8	8.0	139
	4.4.72	0000	101.25	251	1.406	365.0	5.5	112
	4.4.72	0600	101.16	250	1.410	273.0	7.4	102
	4.4.72	1200	101.14	246	1.433	139.3	14.2	71
	4.4.72	1800	101.17	248	1.421	390.1	5.1	89
	5.4.72	0000	101.36	251	1.407	356.6	5.7	65
	10.4.72	0000	101.31	253	1.395	847.0	2.4	163
	10.4.72	0600	101.12	250	1.409	721.6	2.8	133
	12.4.72	0600	101.35	251	1.407	231.3	8.7	122
	12.4.72	1200	100.99	248	1.419	236.8	8.5	105
	12.4.72	1800	100.67	252	1.392	156.0	13.1	101
	13.4.72	0000	100.35	254	1.377	178.3	11.6	9
	13.4.72	0600	99.92	253	1.376	175.5	11.8	99
	13.4.72	1200	100.25	256	1.364	170.0	12.2	92
	13.4.72	1800	100.50	254	1.379	147.7	13.9	95
	14.4.72	0000	100.49	256	1.368	125.4	16.6	86
	14.4.72	0600	100.21	256	1.364	222.9	9.3	92
	17.4.72	1800	102.22	252	1.413	261.9	7.7	89
	18.4.72	0000	102.02	254	1.399	167.2	12.1	91
	18.4.72	0600	101.89	254	1.398	130.9	15.5	88

*Site Location see Table 2.2

TABLE B1.4

SITE NO. 6

Site No.*	Date	GMT	p kPa	T_a ^0K	ρ_a $kg\ m^{-3}$	Δn $10^3 m$	$G_{0_{-1}}$ $m\ s^{-1}$	θ_{G_0} Deg.
6	19.7.72	0000	101.65	274	1.293	427.6	5.0	281
	19.7.72	0600	100.79	276	1.272	176.7	12.3	258
	19.7.72	1200	100.81	276	1.273	94.1	23.1	253
	21.7.72	1200	101.09	275	1.281	513.6	4.2	291
	21.7.72	1800	100.89	276	1.274	279.9	7.8	270
	23.7.72	1200	101.13	276	1.277	125.4	17.3	286
	23.7.72	1800	101.42	277	1.276	276.5	7.9	265
	24.7.72	0000	101.85	274	1.295	142.7	11.6	260

*Site Location see Table 2.2

APPENDIX B2

VALUES OF U, G, U_i AND ΔT

U surface wind speed at 10m above the surface

G geostrophic wind speed

U_i estimates of U ($i = 1, 2, 3$)

ΔT air - ice temperature difference

TABLE B2.1

SITE NO. 2

Site No.*	U $m\ s^{-1}$	G $m\ s^{-1}$	U_1 $m\ s^{-1}$	U_2 $m\ s^{-1}$	U_3 $m\ s^{-1}$	ΔT ^0C
2	7.7	7.5	5.7	6.4	5.9	-0.66
	7.0	7.0	5.5	6.2	5.4	0.27
	8.4	6.5	5.2	5.9	5.3	-0.39
	7.8	6.4	5.1	5.9	5.1	0.17
	7.5	8.9	6.5	7.2	6.7	-1.21
	6.7	12.5	8.4	9.0	8.6	-0.86
	9.7	11.4	7.8	8.4	7.5	1.25
	6.6	8.0	6.0	6.7	4.3	8.45
	8.2	13.3	8.9	9.4	8.7	0.72
	8.6	10.3	7.2	7.9	7.5	-1.22
	7.7	9.2	6.6	7.3	6.5	0.48
	6.2	8.4	6.2	6.9	5.7	2.67
	6.0	10.0	7.1	7.7	6.7	1.71
	9.6	14.4	9.5	10.0	9.3	0.50
	16.4	35.5	20.8	20.8	20.8	0.00
	9.9	29.0	17.3	17.5	17.1	0.53
	8.4	25.6	15.5	15.7	14.3	2.88
	5.3	20.4	12.7	13.1	11.9	2.19
	7.3	18.2	11.5	11.9	11.6	-0.15
	10.2	12.5	8.4	9.0	9.5	-4.23

*Site Location see Table 2.2

TABLE B2.2

SITE NOS. 4a AND 4b

Site No.*	U $m\ s^{-1}$	G $m\ s^{-1}$	U_1 $m\ s^{-1}$	U_2 $m\ s^{-1}$	U_3 $m\ s^{-1}$	ΔT ^0C
4a	5.8	7.7	5.8	6.9	8.0	-11.19
	6.6	8.4	6.2	7.3	6.9	- 3.34
	5.5	7.5	5.7	6.8	8.4	-13.82
	4.4	8.1	6.1	7.1	6.1	0.00
	9.2	13.7	9.1	10.6	4.1	18.49
	9.8	13.6	9.0	10.6	4.6	16.38
	9.9	13.5	9.0	10.5	0.2	32.73
	10.1	12.0	8.2	9.6	0.1	32.47
	8.4	6.5	5.2	6.1	7.8	-14.27
4b	3.7	4.7	4.2	5.0	4.8	- 3.39
	4.3	4.9	4.3	5.1	3.8	3.05
	5.7	5.7	4.8	5.6	6.0	- 7.06
	5.3	6.2	5.0	5.9	6.4	- 7.46
	5.8	7.1	5.5	6.5	8.0	-13.00
	6.4	8.6	6.3	7.4	8.0	- 7.98
	5.3	7.6	5.8	6.8	4.9	4.56

*Site Location see Table 2.2

TABLE B2.3

SITE NO. 5

Site No.*	U $m\ s^{-1}$	G $m\ s^{-1}$	U_1 $m\ s^{-1}$	U_2 $m\ s^{-1}$	U_3 $m\ s^{-1}$	ΔT ^{o}C
5	6.7	12.7	8.5	10.1	8.9	-1.35
	6.4	10.0	7.1	8.3	6.2	3.98
	6.4	9.1	6.6	7.8	5.8	3.72
	6.8	8.9	6.5	7.7	5.6	4.20
	6.6	7.0	5.5	6.5	5.8	-1.55
	6.6	6.3	5.1	6.0	5.4	-1.91
	6.3	5.9	4.9	5.8	5.0	-0.61
	6.8	6.6	5.2	6.2	5.0	1.45
	5.8	9.9	7.0	8.3	6.5	2.42
	5.9	10.8	7.5	8.9	6.8	2.88
	7.0	5.4	4.6	5.5	5.1	-2.88
	5.1	5.6	4.7	5.6	5.4	-3.82
	3.4	2.5	3.0	3.6	2.8	1.61
	7.4	8.6	6.3	7.5	7.9	-7.78
	9.8	12.5	8.4	9.9	8.8	-1.48
	10.2	12.0	8.2	9.6	8.6	-1.88
	11.0	11.7	8.0	9.4	7.8	0.62
	10.2	12.0	8.2	9.6	7.3	3.52
	10.1	14.7	9.6	11.3	9.5	0.26
	9.5	15.9	10.3	12.1	10.3	0.00
	7.6	11.0	7.6	9.0	8.3	-3.03
	7.2	12.6	8.5	10.0	9.0	-2.04
	7.3	13.0	8.7	10.2	9.2	-1.95
	6.9	13.9	9.2	10.8	10.9	-6.16

*Site Location see Table 2.2

TABLE B2.4

SITE NO. 6

Site No.*	U $m\ s^{-1}$	G $m\ s^{-1}$	U_1 $m\ s^{-1}$	U_2 $m\ s^{-1}$	U_3 $m\ s^{-1}$	ΔT ^0C
6	5.9	5.5	4.7	5.5	4.7	0:00
	9.1	7.7	5.8	6.9	5.4	2.21
	8.4	10.0	7.1	8.4	6.2	3.75
	9.7	11.6	7.9	9.4	6.3	6.70
	14.6	13.9	9.2	10.9	7.6	5.71
	13.7	15.5	10.0	11.9	7.8	7.82
	12.3	17.5	11.1	13.2	9.9	4.05
	14.1	18.7	11.8	14.0	10.0	5.33
	8.9	5.4	4.6	5.5	4.0	3.68
	10.0	7.2	5.6	6.6	4.2	7.34
	6.1	7.6	5.8	6.9	4.9	4.25
	9.6	10.1	7.1	8.5	6.4	3.17
	3.3	8.7	6.4	7.6	5.9	2.50
	9.7	6.9	5.4	6.4	4.7	3.92
	10.5	5.4	4.6	5.5	4.0	3.51
	9.8	7.9	5.9	7.1	5.7	1.06

*Site Location see Table 2.2

APPENDIX C

GEOSTROPHIC WIND VELOCITY DATA

P_1 atmospheric pressure

T_{a1} air temperature

$\rho_{a1,2}$ air density

Δn_1 distance between adjacent isobars

$G_{1,2}$ geostrophic wind speed

$\theta_{G1,2}$ geostrophic wind direction

$_1$ denotes quantities measured or derived from measurements on surface weather charts

$_2$ denotes quantities obtained from linear interpolation on $_1$.

TABLE C1

CYCLE NO. 21

Date	GMT	p_1 kPa	T_a ^0K	ρa_1 kg m^{-3}	ρa_2 kg m^{-3}	Δn_1 $10^3 m$	G_1 $m\ s^{-1}$	G_2 $m\ s^{-1}$	θG_1 Deg.	θG_2 Deg.
	1800	100.82	275	1.28	1.28	143.2	15.9	15.9	272	272
23.7.73	0000	-	275	-	1.28	-	-	9.4	-	251
	0600	100.73	275	1.28	1.28	779.1	2.9	2.9	230	230
	1200	-	273	-	1.28	-	-	4.3	-	221
	1800	-	278	-	1.28	-	-	5.7	-	211
24.7.73	0000	-	278	-	1.28	-	-	7.1	-	202
	0600	-	281	-	1.28	-	-	8.6	-	193
	1200	-	279	-	1.27	-	-	10.0	-	183
	1800	102.00	279	1.27	1.27	-	-	11.4	174	174
25.7.73	0000	102.18	282	1.26	1.26	178.9	12.8	12.8	168	168
	0600	101.68	281	1.26	1.26	140.4	16.4	16.4	167	167
	1200	-	278	-	1.24	-	-	12.6	-	187
	1800	101.41	291	1.21	1.21	275.3	8.7	8.7	206	206
26.7.73	0000	101.37	298	1.19	1.19	385.4	6.3	6.3	200	200
	0600	101.20	285	1.24	1.24	-	-	6.8	167	167
	1200	-	285	-	1.23	-	-	7.3	-	167
	1800	100.80	288	1.22	1.22	-	-	7.7	166	166
27.7.73	0000	100.82	289	1.22	1.22	289.1	8.2	8.2	187	187
	0600	100.81	287	1.22	1.22	440.5	5.4	5.4	202	202
	1200	-	287	-	1.22	-	-	5.7	-	137
	1800	-	285	-	1.22	-	-	6.1	-	72
28.7.73	0000	101.72	292	1.21	1.21	374.4	6.4	6.4	7	7
	0600	-	284	-	1.22	-	-	7.5	-	49
	1200	101.61	283	-	1.22	-	-	8.7	90	90
	1800	101.34	287	1.23	1.23	239.5	9.8	9.8	130	130
29.7.73	0000	101.18	290	1.22	1.22	159.7	14.9	14.9	120	120

TABLE C2

CYCLE NO.26a

Date	GMT	p_1 kPa	T_a °K	ρa_1 kg m^{-3}	ρa_2 kg m^{-3}	Δn_1 10^{-3}m	G_1 $m\ s^{-1}$	G_2 $m\ s^{-1}$	θ_{G_1} Deg.	θ_{G_2} Deg.
	1800	101.96	260	1.37	1.37	173.2	12.3	12.3	138	138
23.10.73	0000	101.59	265	1.34	1.34	621.3	3.5	3.5	147	147
	0600	101.60	263	1.35	1.35	340.9	6.3	6.3	134	134
	1200	101.25	262	1.35	1.35	483.8	4.5	4.5	123	123
	1800	-	262	-	1.35	-	-	4.6	-	127
24.10.73	0000	-	263	-	1.35	-	-	4.7	-	130
	0600	-	259	-	1.34	-	-	4.7	-	134
	1200	100.90	261	1.34	1.34	456.3	4.8	4.8	137	137
	1800	100.87	263	1.34	1.34	302.4	7.2	7.2	149	149
25.10.73	0000	100.95	265	1.33	1.33	252.9	8.7	8.7	138	138
	0600	100.91	263	1.34	1.34	368.4	5.9	5.9	136	136
	1200	100.65	264	1.33	1.33	195.2	11.2	11.2	149	149
	1800	100.43	263	1.33	1.33	280.4	7.8	7.8	165	165
26.10.73	0000	100.03	270	1.24	1.24	233.7	9.7	9.7	152	152
	0600	99.82	265	1.31	1.31	335.4	6.6	6.6	167	167
	1200	99.66	263	1.32	1.32	288.6	7.6	7.6	154	154
	1800	-	265	-	1.32	-	-	7.2	-	158
27.10.73	0000	-	263	-	1.33	-	-	6.7	-	162
	0600	-	-	-	1.33	-	-	6.3	-	165
	1200	-	261	-	1.33	-	-	5.8	-	169
	1800	-	262	-	1.33	-	-	5.4	-	173
28.10.73	0000	-	-	-	1.34	-	-	4.9	-	177
	0600	-	260	-	1.34	-	-	4.5	-	180
	1200	99.60	259	1.34	1.34	-	-	4.0	184	184
	1800	-	261	-	1.33	-	-	3.6	-	204
29.10.73	0000	99.80	265	1.31	1.31	725.7	3.1	3.1	223	223

TABLE C3

CYCLE NO. 26b

Date	GMT	p_1 kPa	T_a ^0K	ρ_{a_1} kg m^{-3}	ρ_{a_2} kg m^{-3}	Δn_1 10^3m	G_1 m s^{-1}	G_2 m s^{-1}	θ_{G1} Deg.	θ_{G2} Deg.
	1800	100.70	264	1.33	1.33	584.7	3.8	3.8	165	165
25.10.73	0000	-	264	-	1.33	-	-	7.9	-	157
	0600	100.61	263	1.33	1.33	183.9	11.9	11.9	149	149
	1200	-	-	-	1.33	-	-	10.3	-	161
	1800	-	262	-	1.32	-	-	8.7	-	174
26.10.73	0000	99.75	265	1.31	1.31	315.7	7.1	7.1	186	186
	0600	99.65	264	1.32	1.32	436.4	5.1	5.1	209	209
	1200	99.46	264	1.31	1.31	543.5	4.1	4.1	196	196
	1800	-	263	-	1.31	-	-	5.5	-	233
27.10.73.	0000	-	264	-	1.31	-	-	6.9	-	271
	0600	99.47	265	1.31	1.31	269.0	8.3	8.3	308	308
	1200	-	262	-	1.31	-	-	7.5	-	300
	1800	-	261	-	1.32	-	-	6.7	-	292
28.10.73	0000	-	262	-	1.32	-	-	5.9	-	284
	0600	-	259	-	1.33	-	-	5.0	-	276
	1200	-	260	-	1.33	-	-	4.2	-	268
	1800	-	-	-	1.34	-	-	3.4	-	260
29.10.73.	0000	99.77	259	1.34	1.34	831.7	2.6	2.6	252	252
	0600	-	261	-	1.34	-	-	4.6	-	271
	1200	-	262	-	1.34	-	-	6.6	-	290
	1800	-	260	-	1.34	-	-	8.7	-	310
30.10.73	0000	-	264	-	1.33	-	-	10.7	-	329
	0600	100.93	264	1.33	1.33	172.9	12.7	12.7	348	348
	1200	101.34	261	1.35	1.35	167.4	12.9	12.9	344	344
	1800	-	260	-	-	-	-	-	-	-
31.10.73	0000	-	260	-	-	-	-	-	-	-

TABLE C4

CYCLE NO. 41

Date	GMT	p_1 kPa	T_a ^0K	ρ_{a_1} kg m^{-3}	ρ_{a_2} kg m^{-3}	Δn_1 10^3m	G_1 m s^{-1}	G_2 m s^{-1}	θ_{G_1} Deg.	θ_{G_2} Deg.
	1800	101.10	275	1.28	1.28	258.0	8.8	8.8	87	87
23.7.74	0000	100.94	275	1.28	1.28	172.9	13.2	13.2	92	92
	0600	101.03	274	1.29	1.29	181.2	12.5	12.5	92	92
	1200	100.99	274	1.28	1.28	271.7	8.4	8.4	92	92
	1800	-	277	-	1.27	-	-	8.7	-	95
24.7.74	0000	100.89	280	1.26	1.26	258.0	9.0	9.0	97	97
	0600	100.91	275	1.28	1.28	491.3	4.6	4.6	97	97
	1200	100.97	276	1.28	1.28	430.9	5.3	5.3	100	100
	1800	100.97	278	1.27	1.27	400.8	5.8	5.8	113	113
25.7.74	0000	101.18	277	1.27	1.27	219.6	10.4	10.4	117	117
	0600	-	278	-	1.27	-	-	9.9	-	126
	1200	-	276	-	1.27	-	-	9.3	-	134
	1800	-	278	-	1.27	-	-	8.8	-	143
26.7.74	0000	-	277	-	1.27	-	-	8.2	-	152
	0600	-	278	-	1.27	-	-	7.7	-	160
	1200	-	275	-	1.26	-	-	7.2	-	169
	1800	-	278	-	1.26	-	-	6.6	-	177
27.7.74	0000	-	280	-	1.26	-	-	6.1	-	186
	0600	-	279	-	1.26	-	-	5.5	-	195
	1200	-	277	-	1.26	-	-	5.0	-	203
	1800	101.77	282	1.26	1.26	516.0	4.5	4.5	212	212
28.7.74	0000	101.57	281	1.26	1.26	417.2	5.6	5.6	221	221
	0600	101.48	279	1.27	1.27	447.4	5.1	5.1	205	205
	1200	-	286	-	1.24	-	-	7.6	-	217
	1800	100.84	291	1.21	1.21	238.8	10.1	10.1	228	228
29.7.74	0000	100.78	293	1.20	1.20	203.1	12.0	12.0	240	240

TABLE C5

CYCLE NO. 43

Date	GMT	p_1 kPa	T_a ^0K	ρ_{a_1} kg m^{-3}	ρ_{a_2} kg m^{-3}	Δn_1 10^3m	G_1 m s^{-1}	G_2 m s^{-1}	θ_{G_1} Deg.	θ_{G_2} Deg.
	1800	102.8	273	1.31	1.31	-	-	-	88	88
23.8.74	0000	-	-	-	1.31	-	-	-	-	97
	0600	-	275	-	1.30	-	-	-	-	106
	1200	102.17	274	1.30	1.30	184.2	12.2	12.2	115	115
	1800	-	274	-	1.29	-	-	12.8	-	123
24.8.74	0000	101.90	278	1.28	1.28	170.4	13.4	13.4	131	131
	0600	101.31	276	1.28	1.28	241.9	9.4	9.4	142	142
	1200	-	274	-	1.26	-	-	10.3	-	148
	1800	101.11	283	1.25	1.25	208.9	11.2	11.2	153	153
25.8.74	0000	101.02	283	1.24	1.24	338.1	6.9	6.9	159	159
	0600	-	279	-	1.26	-	-	8.2	-	158
	1200	100.89	278	1.27	1.27	244.7	9.4	9.4	156	156
	1800	100.96	277	1.27	1.27	206.2	11.1	11.1	154	154
26.8.74	0000	101.25	276	1.28	1.28	219.9	10.4	10.4	144	144
	0600	101.10	274	1.29	1.29	321.6	7.0	7.0	149	149
	1200	101.20	275	1.28	1.28	-	-	8.5	143	143
	1800	101.23	278	1.27	1.27	230.9	9.9	9.9	147	147
27.8.74	0000	-	278	-	1.27	-	-	10.0	-	147
	0600	-	279	-	1.27	-	-	10.1	-	148
	1200	-	276	-	1.27	-	-	10.1	-	148
	1800	-	279	-	1.27	-	-	10.2	-	149
28.8.74	0000	101.39	279	1.27	1.27	222.7	10.3	10.3	149	149
	0600	101.11	280	1.26	1.26	343.6	6.7	6.7	159	159
	1200	-	273	-	-	-	-	-	-	-
	1800	-	286	-	-	-	-	-	-	-
29.8.74	0000	-	-	-	-	-	-	-	-	-

TABLE C6

CYCLE NO. 60

Date	GMT	p_1 kPa	T_a ^0K	ρ_{a2} kg m^{-3}	ρ_{a2} kg m^{-3}	Δn_1 10^3m	G_1 m s^{-1}	G_2 m s^{-1}	θ_{G1} Deg.	θ_{G2} Deg.
	1800	101.14	278	1.27	1.27	212.0	10.8	10.8	149	149
23.6.75	0000	100.88	279	1.26	1.26	143.2	16.1	16.1	155	155
	0600	100.46	276	1.27	1.27	140.4	16.3	16.3	156	156
	1200	100.25	280	1.25	1.25	178.9	13.0	13.0	152	152
	1800	100.03	281	1.24	1.24	190.0	12.3	12.3	147	147
24.6.75	0000	-	282	-	1.24	-	-	11.0	-	125
	0600	-	-	-	1.23	-	-	9.6	-	103
	1200	-	286	-	1.23	-	-	8.3	-	82
	1800	-	282	-	1.23	-	-	6.9	-	60
25.6.75	0000	100.41	286	1.22	1.22	421.2	5.6	5.6	38	38
	0600	100.54	286	1.23	1.23	272.6	8.7	8.7	57	57
	1200	-	281	-	1.24	-	-	9.4	-	66
	1800	-	283	-	1.25	-	-	10.1	-	75
26.6.75	0000	-	-	-	1.25	-	-	10.8	-	83
	0600	-	283	-	1.26	-	-	11.5	-	92
	1200	101.26	277	1.27	1.27	187.2	12.2	12.2	101	101
	1800	101.48	287	1.24	1.24	272.6	8.6	8.6	119	119
27.6.75	0000	101.47	280	1.26	1.26	264.3	8.7	8.7	122	122
	0600	101.50	280	1.26	1.26	388.2	5.9	5.9	120	120
	1200	-	284	-	1.26	-	-	5.9	-	120
	1800	-	278	-	1.27	-	-	5.8	-	121
28.6.75	0000	-	279	-	1.27	-	-	5.8	-	121
	0600	-	277	-	1.27	-	-	5.7	-	121
	1200	-	277	-	1.27	-	-	5.7	-	122
	1800	101.53	278	1.27	1.27	401.9	5.7	5.7	122	122
29.6.75	0000	-	277	-	-	-	-	-	-	-

APPENDIX D

TIME ADJUSTED GEOSTROPHIC WIND VELOCITY DATA

t_1 mean scanning time of LANDSAT-1 image

ρ_a air density

G_3 geostrophic wind speed

θ_{G_3} geostrophic wind direction

$_3$ denotes quantities adjusted to LANDSAT-1 mean scanning time.

TABLE D1

CYCLE NO. 21

t_i	Date	GMT	ρ_{a_3} kg m^{-3}	G_3 $m\,s^{-1}$	θ_{G_3} Deg.
-	22.7.73	195610	1.28	13.8	265
		015735	1.28	7.3	244
		075900	1.28	3.4	227
		140025	1.28	4.8	218
-	23.7.73	200150	1.28	6.2	208
		020315	1.28	7.6	199
		080414	1.28	9.1	190
		140605	1.27	10.5	180
t_1	24.7.73	200730	1.27	11.9	172
		020858	1.26	14.1	168
		081025	1.25	15.0	174
		141153	1.23	11.2	194
t_2	25.7.73	201320	1.20	7.8	204
		021445	1.21	6.5	188
		081610	1.24	7.0	167
		141735	1.23	7.5	167
t_3	26.7.73	201900	1.22	7.9	174
		022025	1.22	7.1	193
		082150	1.22	5.5	176
		142315	1.22	5.9	111
t_4	27.7.73	202440	1.22	6.2	46
		022605	1.21	6.8	24
		082730	1.22	8.0	66
		142855	1.22	9.2	107
t_5	28.7.73	203020	1.23	11.9	126

TABLE D2

CYCLE NO.26a

t_i	Date	GMT	ρ_{a_3} kg m^{-3}	G_3 $m\ s^{-1}$	θ_{G_3} Deg.
-	22.10.73	200630	1.36	9.2	141
		020755	1.34	4.5	142
		080920	1.35	5.7	130
		141045	1.35	4.5	124
t_1	23.10.73	201210	1.35	4.6	128
		021330	1.35	4.7	131
		081450	1.34	4.7	135
		141610	1.34	5.7	142
t_2	24.10.73	201730	1.34	7.8	145
		021855	1.33	7.6	137
		082020	1.34	8.0	141
		142145	1.33	9.9	155
t_3	25.10.73	202310	1.29	8.6	160
		022428	1.27	8.5	158
		082605	1.31	7.0	162
		142733	1.32	7.4	156
t_4	26.10.73	202900	1.32	7.0	160
		023025	1.33	6.5	163
		083150	1.33	6.1	167
		143315	1.33	5.6	171
t_5	27.10.73	203440	1.33	5.2	175
		023608	1.34	4.7	178
		083735	1.34	4.3	182
		143903	1.34	3.8	193
t_6	28.10.73	204030	1.32	3.4	212

TABLE D3

CYCLE NO. 26b

t_i	Date	GMT	ρ_{a_3} $kg\ m^{-3}$	G_3 $m\ s^{-1}$	θ_{G_3} Deg.
-	24.10.73	201800	1.33	5.4	160
		021925	1.33	9.4	154
		082050	1.33	11.3	154
		142115	1.33	9.7	166
t_1	25.10.73	202340	1.32	8.1	179
		022505	1.31	6.3	191
		082730	1.32	4.7	204
		142855	1.31	4.7	211
t_2	26.10.73	202920	1.31	6.1	249
		023048	1.31	7.5	286
		083215	1.31	8.0	305
		143343	1.31	7.2	297
t_3	27.10.73	203510	1.32	6.4	289
		023630	1.32	5.5	281
		083750	1.33	4.7	273
		143910	1.33	3.9	264
t_4	28.10.73	204030	1.34	3.0	256
		024155	1.34	3.5	261
		084320	1.34	5.5	280
		144445	1.34	7.6	299
t_5	29.10.73	204610	1.34	9.6	319

TABLE D4

CYCLE NO. 41

t_i	Date	GMT	ρ_{a_3} $kg\ m^{-3}$	G_3 $m\ s^{-1}$	θ_{G_3} Deg.
-	22.7.74	201730	1.28	10.5	89
		021855	1.28	12.9	92
		082020	1.29	10.9	92
		142145	1.28	8.5	93
-	23.7.74	202310	1.27	8.8	96
		022430	1.27	7.2	97
		082550	1.28	4.9	98
		142710	1.28	5.5	105
t_1	24.7.74	202830	1.27	7.7	115
		022955	1.27	10.2	121
		083120	1.27	9.6	129
		143245	1.27	9.1	138
t_2	25.7.74	203410	1.27	8.5	147
		023535	1.27	8.0	155
		083700	1.27	7.5	164
		143825	1.26	6.9	173
t_3	26.7.74	203950	1.26	6.4	181
		024115	1.26	5.8	190
		084240	1.26	5.3	199
		144405	1.26	4.8	207
t_4	27.7.74	204530	1.26	5.0	216
		024653	1.26	5.4	214
		084815	1.26	6.3	211
		144938	1.23	8.8	222
t_5	28.7.74	205100	1.21	11.0	234

TABLE D5

CYCLE NO. 43

t_i	Date	GMT	ρ_{a_3} $kg\ m^{-3}$	G_3 $m^3\ s^{-1}$	θ_{G_3} Deg.
-	23.8.74	195320	1.29	13.0	126
		015438	1.28	12.1	135
		075555	1.27	9.7	144
		135713	1.26	10.6	150
t_1	24.8.74	195830	1.25	9.8	155
		015958	1.25	7.3	159
		080125	1.26	8.6	157
		140253	1.27	10.0	155
t_2	25.8.74	200420	1.27	10.9	151
		020545	1.28	9.2	146
		080710	1.29	7.5	147
		140835	1.28	9.0	144
t_3	26.8.74	201000	1.27	9.9	147
		021125	1.27	10.0	147
		081250	1.27	10.1	148
		141415	1.27	10.1	148
t_4	27.8.74	201540	1.27	10.2	149

TABLE D6

CYCLE NO. 60

t_i	Date	GMT	ρ_a kg m^{-3}	G_s m s^{-1}	θ_{G_s} Deg.
-	22.6.75	192250	1.27	12.0	150
		012415	1.26	16.1	155
		072540	1.27	15.5	155
		132705	1.25	12.8	151
-	23.6.75	192830	1.24	12.0	142
		012955	1.24	10.7	120
		073120	1.23	9.3	98
		133245	1.23	7.9	76
t_1	24.6.75	193410	1.23	6.6	54
		013535	1.22	6.4	43
		073700	1.23	8.9	59
		133825	1.24	9.6	68
t_2	25.6.75	193950	1.25	10.3	77
		014113	1.25	11.0	86
		074235	1.26	11.7	95
		134358	1.26	11.2	106
t_3	25.6.75	194520	1.25	8.6	120
		014645	1.26	7.9	121
		074810	1.26	5.9	120
		134935	1.26	5.9	120
t_4	27.6.75	195100	1.27	5.8	121

APPENDIX E

LANDSAT-1 MSS IMAGES AVAILABLE AND USED IN THIS STUDY.

TABLE E1

LANDSAT-1 IMAGES RECORDED DURING 1973

25 cloud cover percentage for available frame

25 image selected for study

Cycle #	Row #	+6	+5	+4	+3	+2	+1	Date	0	-1	-2	-3	-4	-5	Days Path#
		76	75	74	73	72	71		70	69	68	67	66	65	
17	9							15. 9							9 17
17	10							15. 5		40					10 17
17	11			50	55			15. 5							11 17
18	9							2. 6							9 18
18	10							2. 6				70			10 18
18	11			30	30			2. 6							11 18
19	9							20. 6					20	5	9 19
19	10							20. 6			15		5	45	10 19
19	11					90	85	20. 6	20		25		35	65	11 19
20	9							8. 7		75	10	35			2 20
20	10	0						8. 7		20		0		95	10 20
20	11						75	8. 7		15		20	10		11 20
21	9	40	75					26. 7	*80*	*25*	*5*	98			9 21
21	10	25			80			26. 7	*30*	*0*	*0*				10 21
21	11			75	35	70		26. 7	0	10	0				11 21
22	9			40				13. 8			40				9 22
22	10				15			13. 8							10 22
22	11			70	35			13. 8			75	75			11 22
23	9						20	31. 8	80	40					9 23
23	10							31. 8	30	60	85				10 23
23	11			35	85	35	5	31. 8	50	35					11 23
24	9							18. 9	60	20					9 24
24	10							18. 9	35	5	75				10 24
24	11						75	18. 9	5	1	0	15			11 24
25	9	35						6. 10						15	9 25
25	10				85			6. 10							10 25
25	11				40	60		6. 10							11 25
26	9				70	70		24. 10							9 26
26	10			*20*	5	*40*	*70*	24. 10	*85*	*99*					10 26
26	11			*10*	*45*	*10*	*5*	24. 10	*20*	*40*					11 26
Path#		76	75	74	73	72	71	Date	70	69	68	67	66	65	Row # Cycle #
Days		+6	+5	+4	+3	+2	+1		0	-1	-2	-3	-4	-5	

TABLE E2

LANDSAT-1 IMAGES RECORDED DURING 1974

25 cloud cover percentage for available frame

25 image selected for study

Cycle #	Row #	+6	+5	+4	+3	+2	+1		0	-1	-2	-3	-4	-5	Days
		76	75	74	73	72	71	Date	70	69	68	67	66	65	Path#
37	9				20			10. 5							9 37
37	10		50					10. 5					1	15	10 37
37	11		10	50	20			10. 5	50	15		0	1	10	11 37
38	9			40				28. 5							9 38
38	10							28. 5		25					10 38
38	11						35	28. 5	0	0	45				11 38
39	9							15. 6	35						9 39
39	10							15. 6	25	40					10 39
39	11				50			15. 6	15	25	35		10	25	11 39
40	9							3. 7						35	9 40
40	10							3. 7			40				10 40
40	11							3. 7							11 40
41	9		40	25	50	50		21. 7			2	0	0	50	9 41
41	10	*30*	*25*	*40*	*50*	50		21. 7			2	10	0	0	10 41
41	11		25	*30*	*40*			21. 7			20	15	0	5	11 41
42	9			15		45		8. 8	20	35	0	25			9 42
42	10							8. 8	20	45	5	5		20	10 42
42	11					25		8. 8	25	10	5			1	11 42
43	9			25				26. 8	45		5	30		35	9 43
43	10		30	30				26. 8	*0*	*15*	*0*	30			10 43
43	11							26. 8	0	1	2	35	50		11 43
44	9							13. 9							9 44
44	10							13. 9		1	30	15			10 44
44	11							13. 9			10	1			11 44
45	9			10				1. 10				1			9 45
45	10			15				1. 10				25			10 45
45	11		3	47	50			1. 10				25			11 45
46	9							19. 10		50				25	9 46
46	10							19. 10	40					50	10 46
46	11						15	19. 10						35	11 46
Path#		76	75	74	73	72	71	Date	70	69	68	67	66	65	Row # / Cycle #
Days		+6	+5	+4	+3	+2	+1		0	-1	-2	-3	-4	-5	

TABLE E3

LANDSAT-1 IMAGES RECORDED DURING 1975

25 cloud cover percentage for available frame

"5 image selected for study"

Cycle #	Row #	+6	+5	+4	+3	+2	+1	Date	0	-1	-2	-3	-4	-5	Days Path#
		76	75	74	73	72	71		70	69	68	67	66	65	
57	9							5. 5							9 57
57	10							5. 5							10 57
57	11			75				5. 5							11 57
58	9	0						23. 5						25	9 58
58	10	0						23. 5		30				35	10 58
58	11	40		60				23. 5		15				20	11 58
59	9			80		80	75	10. 6					75		9 59
59	10		65					10. 6	80						10 59
59	11		55				80	10. 6				20	40		11 59
60	9						60	28. 6				10	25	40	9 60
60	10					75		28. 6			0	35	5	70	10 60
60	11				80		20	28. 6			0	45	25	40	11 60
61	9					20	15	16. 7		5	30		75	75	9 61
61	10					70	75	16. 7		5	45		55		10 61
61	11					70	30	16. 7	65	0	25	70	80		11 61
62	9			70				3. 8	35	35					9 62
62	10			65				3. 8	70	80					10 62
62	11			5				3. 8							11 62
63	9			65	60			21. 8	60	25	20		50	0	9 63
63	10							21. 8		25	15		15	0	10 63
63	11						45	21. 8		15	75		25	0	11 63
64	9					50		8. 9	10					20	9 64
64	10					80		8. 9	50						10 64
64	11			35		45		8. 9							11 64
65	9							26. 9	50			50			9 65
65	10							26. 9					65		10 65
65	11							26. 9					80	80	11 65
66	9							14. 10				50			9 66
66	10							14. 10				80			10 66
66	11							14. 10							11 66
Path#		76	75	74	73	72	71	Date	70	69	68	67	66	65	Row # / Cycle #
Days		+6	+5	+4	+3	+2	+1		0	-1	-2	-3	-4	-5	

APPENDIX F

LISTS OF LANDSAT-1 IMAGES*

---

* These images were ordered from CCRS and ISIS (Integrated Satellite Information Service, Ltd., Prince Albert, Saskatchewan, Canada).

TABLE F1

LIST OF IMAGES SELECTED FOR STUDY

Frame No.				Date			Frame I.D.					
Path		Row		Cycle	Day	Month	Year	LANDSAT		Days		GMT		MSS
68	-	9	-	21	24.	7.	73	E - 1		366	-	20073	-	5
68	-	10	-	21	24.	7.	73	E - 1		366	-	20080	-	5
69	-	9	-	21	25.	7.	73	E - 1		367	-	20132	-	5
69	-	10	-	21	25.	7.	73	E - 1		367	-	20134	-	5
70	-	9	-	21	26.	7.	73	E - 1		368	-	20190	-	7
70	-	10	-	21	26.	7.	73	E - 1		368	-	20193	-	5
69	-	10	-	26 a	23.	10.	73	E - 1		457	-	20115	-	7
69	-	11	-	26 a	23.	10.	73	E - 1		457	-	20121	-	5
70	-	10	-	26 a	24.	10.	73	E - 1		458	-	20173	-	5
70	-	11	-	26 a	24.	10.	73	E - 1		458	-	20180	-	5
71	-	10	-	26 a	25.	10.	73	E - 1		459	-	20231	-	5
71	-	11	-	26 a	25.	10.	73	E - 1		459	-	20234	-	5
72	-	10	-	26 a	26.	10.	73	E - 1		460	-	20290	-	5
72	-	11	-	25 a	26.	10.	73	E - 1		460	-	20292	-	5

TABLE F1 (Cont'd)

LIST OF IMAGES SELECTED FOR STUDY

Frame No.					Date			Frame I.D.				
Path		Row		Cycle	Day	Month	Year	LANDSAT	Julian Day		GMT	MSS
71	-	11	-	26 b	25.	10.	73	E - 1	459	-	20234	- 5
72	-	11	-	26 b	26.	10.	73	E - 1	460	-	20292	- 5
73	-	11	-	26 b	27.	10.	73	E - 1	461	-	20351	- 5
74	-	10	-	26 b	28.	10.	73	E - 1	462	-	20403	- 5
74	-	11	-	26 b	28.	10.	73	E - 1	462	-	20405	- 4
73	-	10	-	41	24.	7.	74	E - 1	731	-	20283	- 7
73	-	11	-	41	24.	7.	74	E - 1	731	-	20285	- 5
74	-	10	-	41	25.	7.	74	E - 1	732	-	20341	- 6
74	-	11	-	41	25.	7.	74	E - 1	732	-	20344	- 5
75	-	10	-	41	26.	7.	74	E - 1	733	-	20395	- 5
76	-	10	-	41	27.	7.	74	E - 1	734	-	20453	- 5

TABLE F1 (Cont'd)

LIST OF IMAGES SELECTED FOR STUDY

Frame No.			Date			Frame I.D.				
Path	Row	Cycle	Day	Month	Year	LANDSAT	Day	Julian Second	GMT	MSS
68	10	43	24.	8.	74	E - 1	762	-	19583	- 5
68	11	43	24.	8.	74	E - 1	762	-	19590	- 5
69	10	43	25.	8.	74	E - 1	763	-	20042	- 5
70	10	43	26.	8.	74	E - 1	764	-	20100	- 5
66	9	60	24.	6.	75	E - 1	11066	-	19335	- 5
66	10	60	24.	6.	75	E - 1	11066	-	19341	- 5
67	9	60	25.	6.	75	E - 1	11067	-	19393	- 5
67	10	60	25.	6.	75	E - 1	11067	-	19395	- 5
68	9	60	26.	6.	75	E - 1	11068	-	19451	- 5
68	10	60	26.	6.	75	E - 1	11068	-	19453	- 5

TABLE F2

LIST OF IMAGES ENLARGED FOR ICE FLOE AREA MEASUREMENT

Frame No.				Date			Frame I.D.					
Path		Row		Cycle	Day	Month Year	LANDSAT	Day	Julian Day	GMT		MSS
68	-	9	-	21	24.	7. 73	E - 1	366	-	20073	-	7
70	-	10	-	26 a	24.	10. 73	E - 1	458	-	20173	-	7
72	-	11	-	26 b	26.	10. 73	E - 1	460	-	20292	-	5
75	-	10	-	41	26.	7. 74	E - 1	733	-	20395	-	5
70	-	10	-	43	26.	8. 74	E - 1	764	-	20100	-	7
66	-	10	-	60	24.	6. 75	E - 1	11066	-	19341	-	5

APPENDIX G

LANDSAT-1 MSS IMAGE AND LOCATIONS OF ICE FLOES

Figure G1.1 MSS 7 No. 68-9-21 from 24.7.73. Floe Nos. 1-23

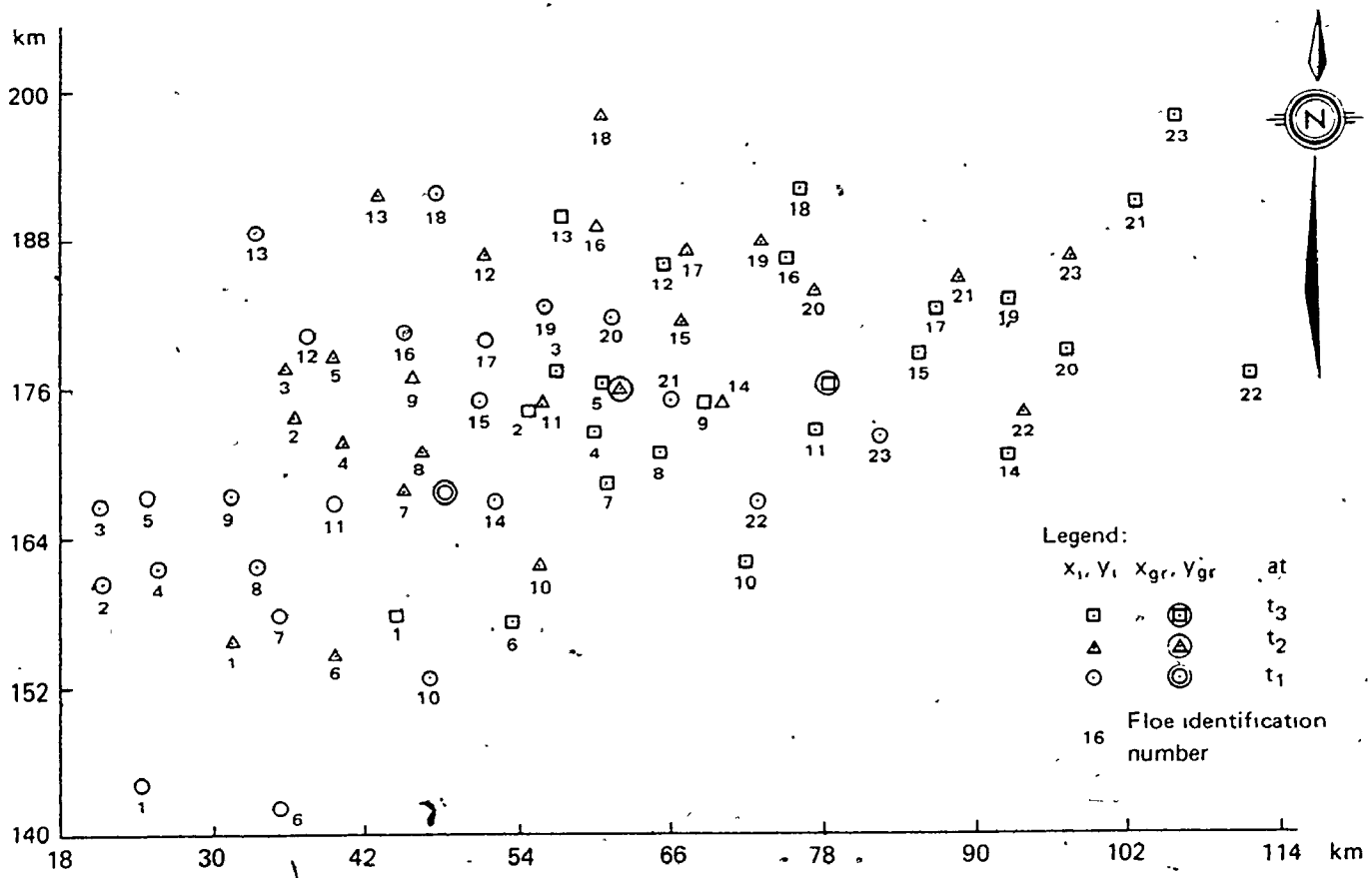

Figure G 1 2 Cycle No. 21 Location of centre of ice floe (x_i, y_i) and centre of gravity of group (x_{gr}, y_{gr}) at mean scanning time (t_i) of LANDSAT – 1 image

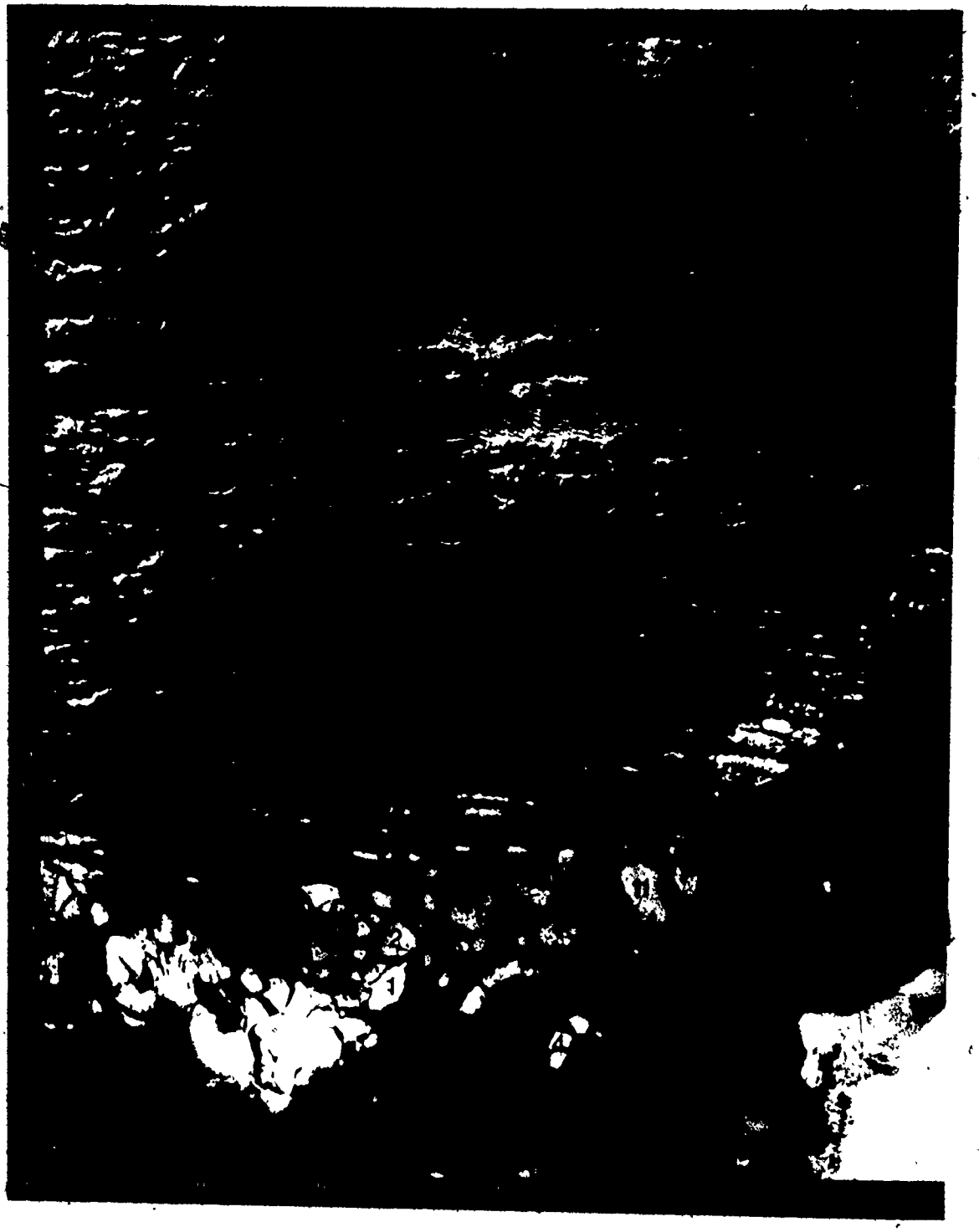

Figure G2.1 MSS 7 No. 70-10-26a from 24.10.73. Floe Nos. 1-12

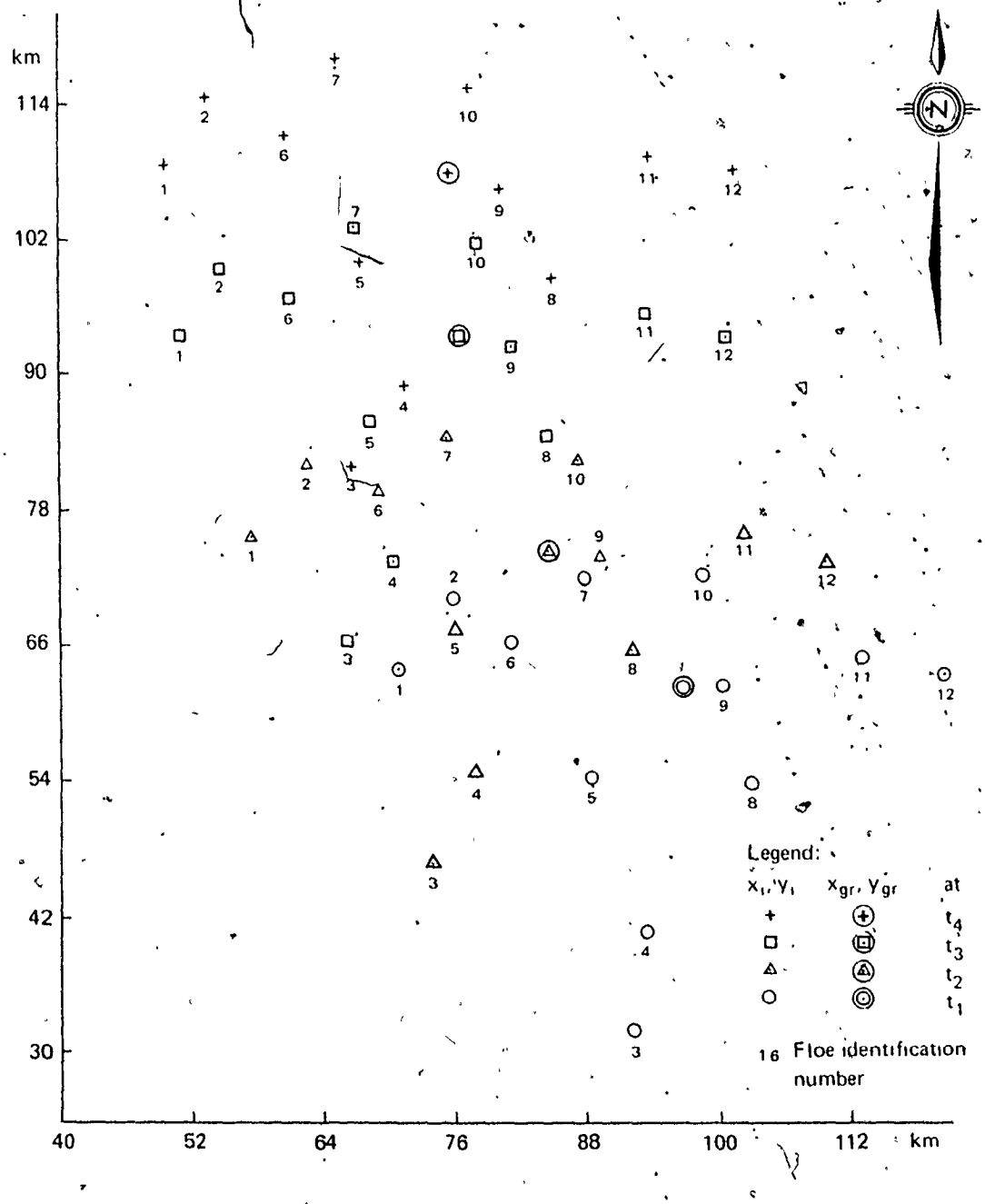

Figure G 2.2 Cycle No. 26 a · Location of centre of ice floe (x_i, y_i) and centre of gravity of group (x_{gr}, y_{gr}) at mean scanning time (t_i) of LANDSAT – 1 image

Figure G3.1 MSS 5 No. 72-11-26b from 26.10.73. Floe Nos. 1-3

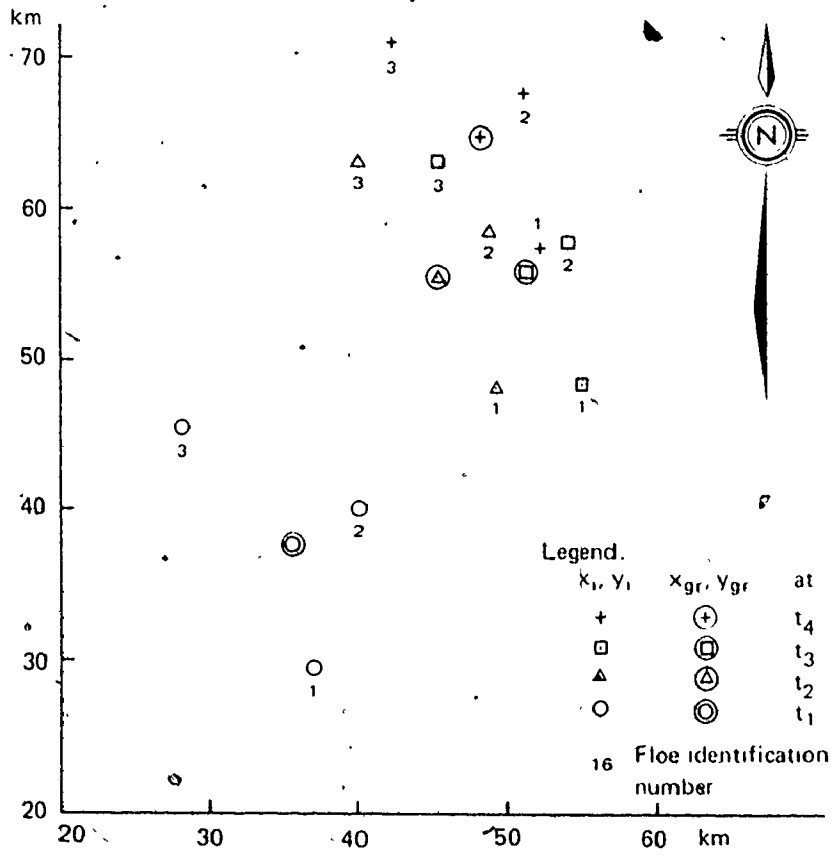

Figure G 3.2 Cycle No. 26b Location of centre of ice floe (x_i, y_i) and centre of gravity of group (x_{gr}, y_{gr}) at mean scanning time (t_i) of LANDSAT – 1 image

Figure G4.1 MSS 7 No. 75-10-41 from 26.7.74. Floe Nos. 1-3

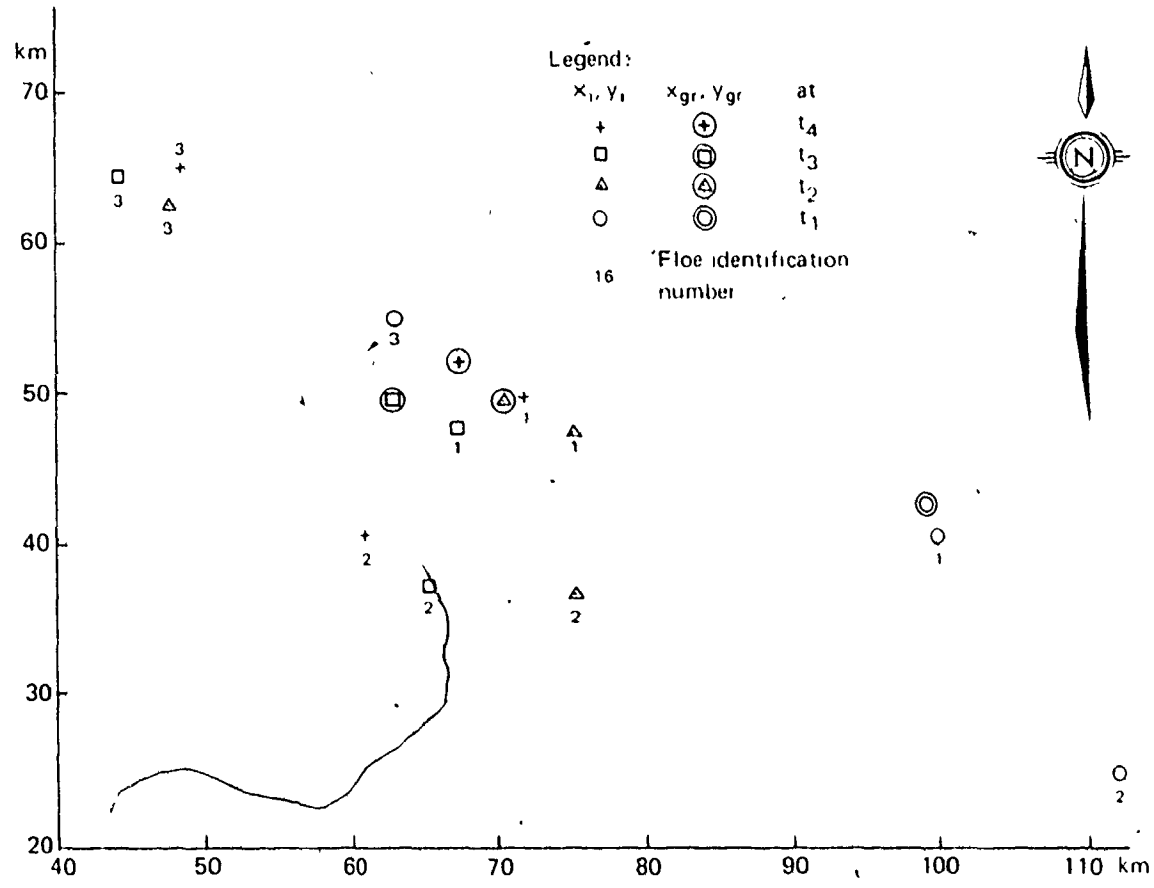

Figure G 4 2 Cycle No. 41 Location of centre of ice floe (x_i, y_i) and centre of gravity of group (x_{gr}, y_{gr}) at mean scanning time (t_i) of LANDSAT – 1 image

Figure G5.1 MSS 7 No. 70-10-43 from 26.8.74. Floe Nos. 1-9

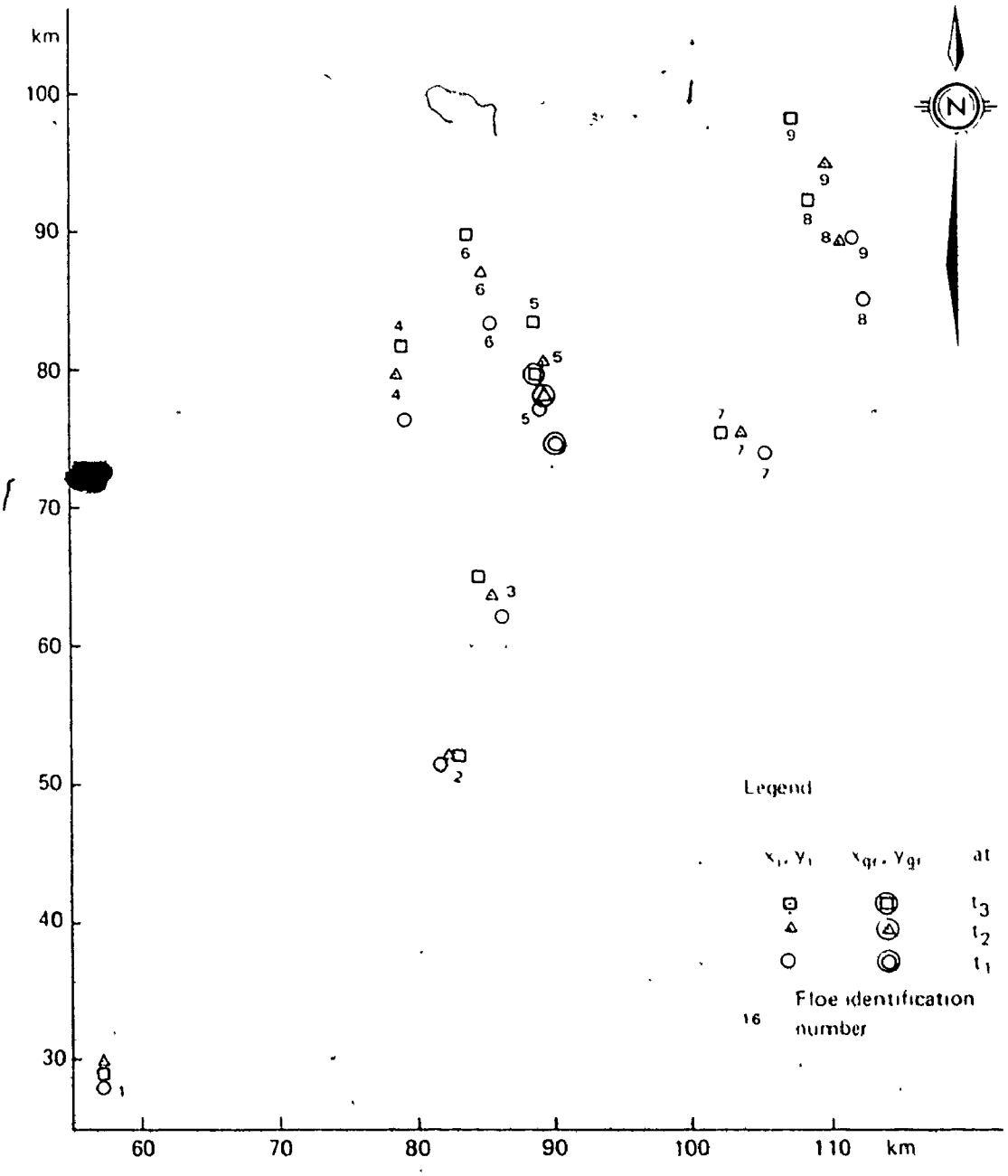

Figure G 5 2 Cycle No. 43 Location of centre of ice floe (x_i, y_i) and centre of gravity of group (x_{gr}, y_{gr}) at mean scanning time (t_i) of LANDSAT – 1 image

Figure G6.1 MSS 7 No. 66-10-60 from 24.6.75. Floe Nos. 1-28

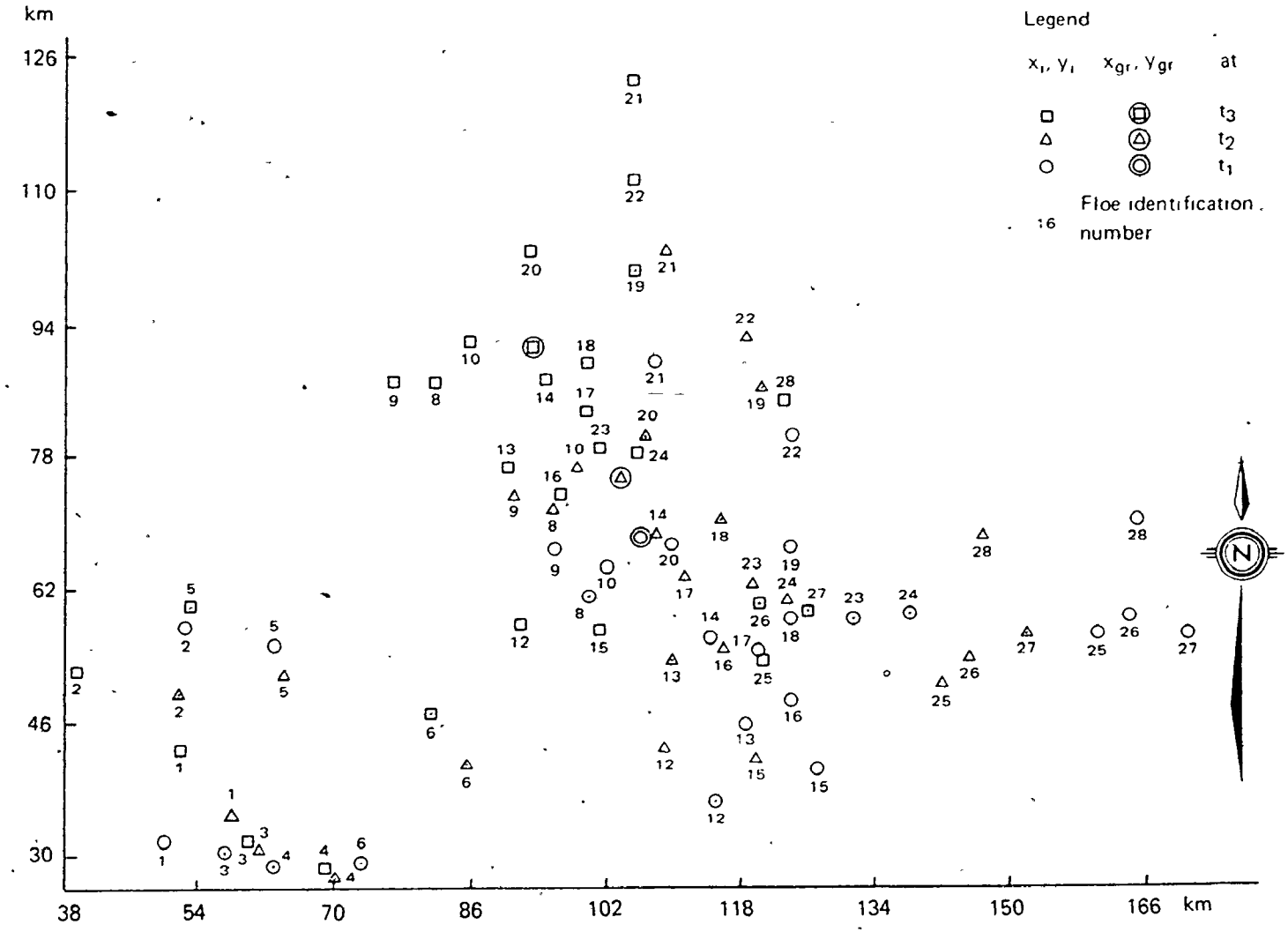

Figure G 6 2 Cycle No. 60 Location of centre of ice floe (x_i, y_i) and centre of gravity of group (x_{gr}, y_{gr}) at mean scanning time (t_i) of LANDSAT – 1 image

APPENDIX H

CO-ORDINATES AND AREA OF AN ICE FLOE

i	I.D. number of a single ice floe in a group
t_i	mean scanning time of LANDSAT-1 image
x_i, y_i	co-ordinate of the geometric centre of a single ice floe
A_i	area of a single ice floe
ΣA_i	area of a group of ice floes.

TABLE H1

CYCLE NO. 21

i	t_1 24.7.73 200730		t_2 25.7.73 201320		t_3 26.7.73 201900		A_i
	x_i 10^3m	y_i 10^3m	x_i 10^3m	y_i 10^3m	x_i 10^3m	y_i 10^3m	10^6m^2
1	24.6	144.8	31.5	155.2	44.2	157.5	45.1
2	21.3	160.3	36.8	173.7	55.1	174.0	6.3
3	20.6	166.4	35.8	177.5	56.9	177.3	8.0
4	25.9	161.3	40.6	171.7	59.7	172.2	13.1
5	24.9	167.1	39.6	178.3	60.7	176.0	6.6
6	35.1	142.2	39.9	154.4	53.8	157.0	9.0
7	35.1	157.5	45.0	167.4	61.0	168.1	9.8
8	33.5	161.5	46.7	170.7	65.0	170.4	13.3
9	31.5	167.1	46.0	176.8	68.6	174.5	43.4
10	47.2	152.4	56.1	161.3	71.9	161.8	172.9
11	39.6	166.6	55.9	174.5	77.5	172.2	25.4
12	37.3	180.3	51.6	186.7	65.5	185.9	29.1
13	33.3	188.5	43.2	191.3	57.9	189.7	57.8
14	52.6	166.6	70.1	174.8	92.5	170.2	51.4
15	51.1	174.8	67.1	181.9	85.6	178.6	22.9
16	45.2	181.4	60.2	188.7	74.9	186.4	23.3
17	51.8	179.8	67.6	186.4	86.9	182.1	4.9
18	47.8	191.5	60.5	197.6	76.2	191.8	26.8
19	56.1	182.6	73.2	187.5	92.5	182.6	47.9
20	61.2	181.4	77.5	183.4	96.8	178.8	14.1
21	66.0	174.8	88.9	184.2	102.4	190.5	29.9
22	72.9	166.6	94.0	173.5	111.3	176.8	52.4
23	82.6	171.5	97.5	186.2	105.4	197.6	67.2
Σ	-	-	-	-	-	-	780.6

TABLE H2

CYCLE NO. 26a

i	t_1 23.10.73 201150		t_2 24.10.73 201730		t_3 25.10.73 202310		t_4 26.10.73 202900		A_i
	x_i 10^3m	y_i 10^3m	x_i 10^3m	y_i 10^3m	x_i 10^3m	y_i 10^3m	x_i 10^3m	y_i 10^3m	10^6m^2
1	70.9	64.0	57.7	75.7	51.1	93.7	49.5	108.7	30.9
2	75.7	70.4	62.2	81.8	54.6	99.3	53.3	114.8	26.4
3	92.2	32.0	74.4	47.2	66.0	66.8	66.8	82.0	40.8
4	93.2	40.9	78.2	54.9	70.4	73.9	71.4	89.2	21.3
5	88.4	53.8	75.9	67.3	68.3	85.9	67.3	100.8	90.4
6	81.3	66.3	69.1	79.5	61.0	97.0	60.5	111.3	30.3
7	87.9	71.9	75.4	84.6	66.8	102.9	65.5	118.1	137.1
8	103.4	53.8	92.5	65.5	83.8	84.6	84.6	98.8	77.3
9	100.3	62.5	89.4	73.7	81.0	92.5	80.8	106.9	67.8
10	98.6	72.4	87.1	82.6	78.0	101.6	77.2	115.8	119.3
11	113.0	65.0	102.4	75.9	93.5	95.3	93.7	109.5	118.9
12	120.4	63.5	109.5	73.7	100.6	93.2	101.1	108.0	49.2
Σ	-	-	-	-	-	-	-	-	809.7

TABLE H3

CYCLE NO. 26b

i	t_1 25.10.73 202340		t_2 26.10.73 202920		t_3 27.10.73 203510		t_4 28.10.73 204030		A_i
	x_i 10^3m	y_i 10^3m	x_i 10^3m	y_i 10^3m	x_i 10^3m	y_i 10^3m	x_i 10^3m	y_i 10^3m	10^6m^2
1	37.1	29.5	49.3	48.0	54.9	48.3	52.3	57.2	28.0
2	39.9	40.1	48.8	58.2	54.1	57.9	51.3	67.8	13.4
3	31.8	45.5	40.1	63.0	45.6	63.0	42.2	71.1	25.2
Σ	-	-	-	-	-	-	-	-	66.6

TABLE H4

CYCLE NO. 41

i	t_1 24. 7.74 202830		t_2 25. 7.74 203410		t_3 26. 7.74 203950		t_4 27. 7.74 204530		A_i
	x_i 10^3m	y_i 10^3m	x_i 10^3m	y_i 10^3m	x_i 10^3m	y_i 10^3m	x_i 10^3m	y_i 10^3m	10^6m^2
1	99.8	40.6	75.2	47.2	67.8	47.2	71.9	49.8	223.8
2	112.3	24.6	75.7	36.8	65.8	37.1	61.0	40.4	13.1
3	63.0	54.9	48.0	62.2	44.5	64.3	48.8	65.0	49.6
Σ	-	-	-	-	-	-	-	-	286.5

TABLE H5

CYCLE NO. 43

i	t_1 24.8.74 195830		t_2 25.8.74 200420		t_3 26.8.74 201000		A_i
	x_i 10^3m	y_i 10^3m	x_i 10^3m	y_i 10^3m	x_i 10^3m	y_i 10^3m	10^6m^2
1	2457.5	2528.3	2457.5	2529.1	2457.5	2528.8	1.2
2	2481.8	2551.4	2482.3	2551.9	2482.9	2551.9	19.0
3	2486.4	2562.1	2485.6	2563.6	2484.6	2564.9	22.1
4	2479.3	2576.3	2478.8	2579.6	2479.0	2581.7	56.5
5	2489.2	2577.1	2489.2	2580.4	2488.7	2583.4	26.8
6	2485.4	2583.2	2484.9	2587.0	2483.9	2589.8	26.8
7	2505.7	2574.0	2503.7	2575.3	2502.4	2575.3	21.9
8	2512.8	2585.0	2511.0	2589.3	2508.8	2592.1	15.4
9	2511.8	2589.5	2510.0	2594.9	2507.5	2598.2	16.8
Σ	-	-	-	-	-	-	206.5

TABLE H6

CYCLE NO. 60

i	t_1 24.6.75 193410		t_2 25.6.75 193950		t_3 26.6.75 194530		A_i
	x_i 10^3m	y_i 10^3m	x_i 10^3m	y_i 10^3m	x_i 10^3m	y_i 10^3m	10^6m^2
1	2549.9	31.8	2557.8	34.5	2552.4	42.4	10.0
2	2552.2	57.4	2551.7	49.0	2539.2	52.3	17.7
3	2557.0	30.2	2561.1	30.2	2559.8	31.0	6.7
4	25631	28.2	2569.5	27.7	2569.0	28.2	78.8
5	2562.9	55.4	2564.4	51.6	2552.7	60.2	218.8
6	2573.0	29.0	2585.7	40.6	2581.9	46.5	8.8
8	2599.9	61.0	2596.1	71.4	2581.8	87.1	21.2
9	2595.9	66.5	2591.3	73.4	2577.2	86.4	12.4
10	2602.5	64.3	2598.7	76.2	2586.2	91.6	9.6

TABLE 116 (Cont'd)

CYCLE NO. 60

i	t_1 24.6.75 193410		t_2 25.6.75 193950		t_3 26.6.75 194530		A_i
	x_i 10^3m	y_i 10^3m	x_i 10^3m	y_i 10^3m	x_i 10^3m	y_i 10^3m	10^6m^2
12	2615.2	36.1	2609.1	42.7	2591.6	57.7	63.6
13	2618.7	45.7	2609.9	53.6	2590.7	76.2	34.2
14	2614.7	55.9	2608.3	68.8	2595.1	87.1	15.9
15	2627.4	40.1	2620.0	41.4	2601.0	56.6	22.0
16	2624.1	48.5	2616.2	54.4	2596.6	73.3	13.0
17	2620.3	54.6	2611.4	64.5	2599.4	83.1	22.8
18	2624.3	58.2	2615.4	69.6	2599.9	89.4	19.2
19	2624.3	66.3	2620.8	86.1	2605.5	100.8	18.3
20	2609.6	67.3	2606.5	80.5	2592.8	102.4	13.2
21	2608.3	89.4	2609.3	102.6	2605.3	122.9	570.4
22	2624.3	80.5	2618.5	92.7	2605.0	110.7	94.3
23	2631.2	58.2	2619.2	62.5	2601.2	78.2	18.1
24	2637.8	58.4	2623.6	60.5	2605.3	78.0	11.0
25	2660.7	56.4	2642.1	50.0	2620.3	53.8	17.3
26	2664.0	58.4	2644.6	53.6	2619.5	60.5	13.0
27	2670.8	56.4	2651.8	55.9	2626.1	58.9	25.9
28	2665.0	69.6	2646.7	68.1	2623.3	84.8	103.5
Σ	-	-	-	-	-	-	1459.7

APPENDIX I

CO-ORDINATES OF THE CENTRE OF GRAVITY

t_i mean scanning time of LANDSAT-1 image

X_{gr}, Y_{gr} co-ordinates of the centre of gravity of a group of ice floes.

TABLE II

CYCLE NO. 21

t_i	Date	G M T	X_{gr} 10^3m	Y_{gr} 10^3m
t_1	24. 7. 73	200730	48.6	167.3
t_2	25. 7. 73	201320	62.1	175.7
t_3	26. 7. 73	201900	78.5	176.0

TABLE I2

CYCLE NO. 26a

t_i	Date	G M T	X_{gr} 10^3m	Y_{gr} 10^3m
t_1	23. 10. 73	201150	96.8	62.5
t_2	24. 10. 73	201730	84.7	74.4
t_3	25. 10. 73	202310	76.2	93.2
t_4	26. 10. 73	202900	75.9	107.9

TABLE I3

CYCLE NO. 26b

t_1	Date	G M T	X_{gr} 10^3m	Y_{gr} 10^3m
t_1	25. 10. 73	202340	35.7	37.7
t_2	26. 10. 73	202920	45.7	55.7
t_3	27. 10. 73	203510	51.2	55.8
t_4	28. 10. 73	204030	48.3	64.6

TABLE I4

CYCLE NO. 41

t_1	Date	G M T	X_{gr} 10^3m	Y_{gr} 10^3m
t_1	24. 7. 74	202830	99.1	42.3
t_2	25. 7. 74	203410	70.5	49.3
t_3	26. 7. 74	203950	63.7	49.7
t_4	27. 7. 74	204530	67.4	52.0

TABLE I5

CYCLE NO. 43

t_i	Date	G M T	X_{gr} 10^3m	Y_{gr} 10^3m
t_1	24. 8. 74	195830	2490.2	2574.3
t_2	25. 8. 74	204020	2489.4	2577.6
t_3	26. 8. 74	201000	2488.8	2579.6

TABLE I6

CYCLE NO. 60

t_i	Date	G M T	X_{gr} 10^3m	Y_{gr} 10^3m
t_1	24. 6. 75	193410	2606.7	68.7
t_2	25. 6. 75	193950	26040.0	75.5
t_3	26. 6. 75	194530	2593.6	90.0

APPENDIX J

MEAN VELOCITY OF THE GEOSTROPHIC WIND AND CENTRE OF GRAVITY

$t_{i,i+1}$	(= t_i + 12:02'50") intermediate scanning time of LANDSAT-1 image
t_i	mean scanning time of LANDSAT-1 image
ρ_{a_4}	air density
G_4	geostrophic wind speed
θ_{G_4}	geostrophic wind direction
$_4$	denotes quantities adjusted to LANDSAT-1 intermediate scanning time
V	speed of motion of centre of gravity of drifting group of ice floes
θ_{ice}	direction of motion of centre of gravity of drifting group of ice floes.

TABLE J1

CYCLE NO. 21

$t_{1\,1\,i+1}$	Date	GMT	ρ_{a_4} kg m^{-3}	G_4 m s^{-1}	θ_{G_4} Deg.	V 10^{-2}m s^{-1}	θ_{ice} Deg.
$t_{1\,2}$	25. 7.73	081025	1.24	12.0	182	18.4	238
$t_{2\,3}$	26. 7.73	081610.	1.22	7.3	180	18.9	269
$t_{3\,4}$	27. 7.73	082150	1.22	6.5	140		
$t_{4\,5}$	28. 7.73	082730	1.22	8.4	74		

TABLE J2

CYCLE NO. 26a

$t_{i\,i+1}$	Date	GMT	ρ_{a_4} kg m^{-3}	G_4 m s^{-1}	θ_{G_4} Deg.	V 10^{-2}m s^{-1}	θ_{ice} Deg.
t_{12}	24.10.73	081450	1.34	5.5	136	19.6	134
t_{23}	25.10.73	082020	1.33	8.4	148	23.8	156
t_{34}	26.10.73	082605	1.30	7.7	153	16.9	179
t_{45}	27.10.73	083150	1.33	6.1	167		
t_{56}	28.10.73	083735	1.33	4.3	188		

TABLE J3

CYCLE NO. 26b

$t_{1\,1i+1}$	Date	GMT	ρ_{a_4} kg m^{-3}	G_4 m s^{-1}	θ_{G4} Deg.	V 10^{-2}m s^{-1}	θ_{ice} Deg.
t_{12}	26.10.73	082730	1.31	6.0	207	23.8	209
t_{23}	27.10.73	083215	1.31	7.0	285	6.3	269
t_{34}	28.10.73	083750	1.33	4.7	273	10.6	162
t_{45}	29.10.73	084320	1.34	5.8	283		

TABLE J4

CYCLE NO. 41

$t_{1\,1\,i+1}$	Date	GMT	ρ_{a_4} kg m^{-3}	G_4 m s^{-1}	θ_{G_4} Deg.	V 10^{-2}m s^{-1}	θ_{ice} Deg.
t_{12}	25. 7.74	083120	1.27	9.0	130	34.0	104
t_{23}	26. 7.74	083700	1.27	7.5	164	7.8	94
t_{34}	27. 7.74	084240	1.26	5.5	199	5.1	238
t_{45}	28. 7.74	084815	1.24	7.3	219		

TABLE J5

CYCLE NO. 43

$t_{1\,1\,i+1}$	Date	GMT	ρ_{a_4} kg m^{-3}	G_4 m s^{-1}	θ_{G4} Deg.	V 10^{-2}m s^{-1}	θ_{ice} Deg.
t_{12}	25. 8.74	080125	1.26	9.3	155	3.4	165
t_{23}	26. 8.74	080710	1.28	9.3	147	2.4	164
t_{34}	27. 8.74	081250	1.27	10.1	148		

TABLE J6

CYCLE NO. 60

$t_{1\,1\,i+1}$	Date	GMT	ρ_{a4} kg m^{-3}	G_4 m s^{-1}	θ_{G4} Deg.	V 10^{-2}m s^{-1}	θ_{ice} Deg.
t_{12}	25. 6,75	073700	1.23	8.4	60	8.4	158
t_{23}	26. 6.75	074235	1.25	10.6	97	21.5	146
t_{34}	27. 6.75	074810	1.26	6.8	120		

APPENDIX K

DISPERSION DIAGRAMS OF WIND SPEED DATA

In this appendix, the dispersion diagrams of observed and calculated geostrophic wind speed against surface wind speed at 5 sites over sea ice (Table 2.2) are compared to lines fitted to data that were measured over sea surfaces by Hasse and Wagner (1971) and Hasse (1974a, 1974b). The observed and calculated wind speed data are presented in Table 2.3. The slopes of Hasse's lines were obtained as geometric means between the regressions of the surface wind speed on the geostrophic wind speed and vice versa.

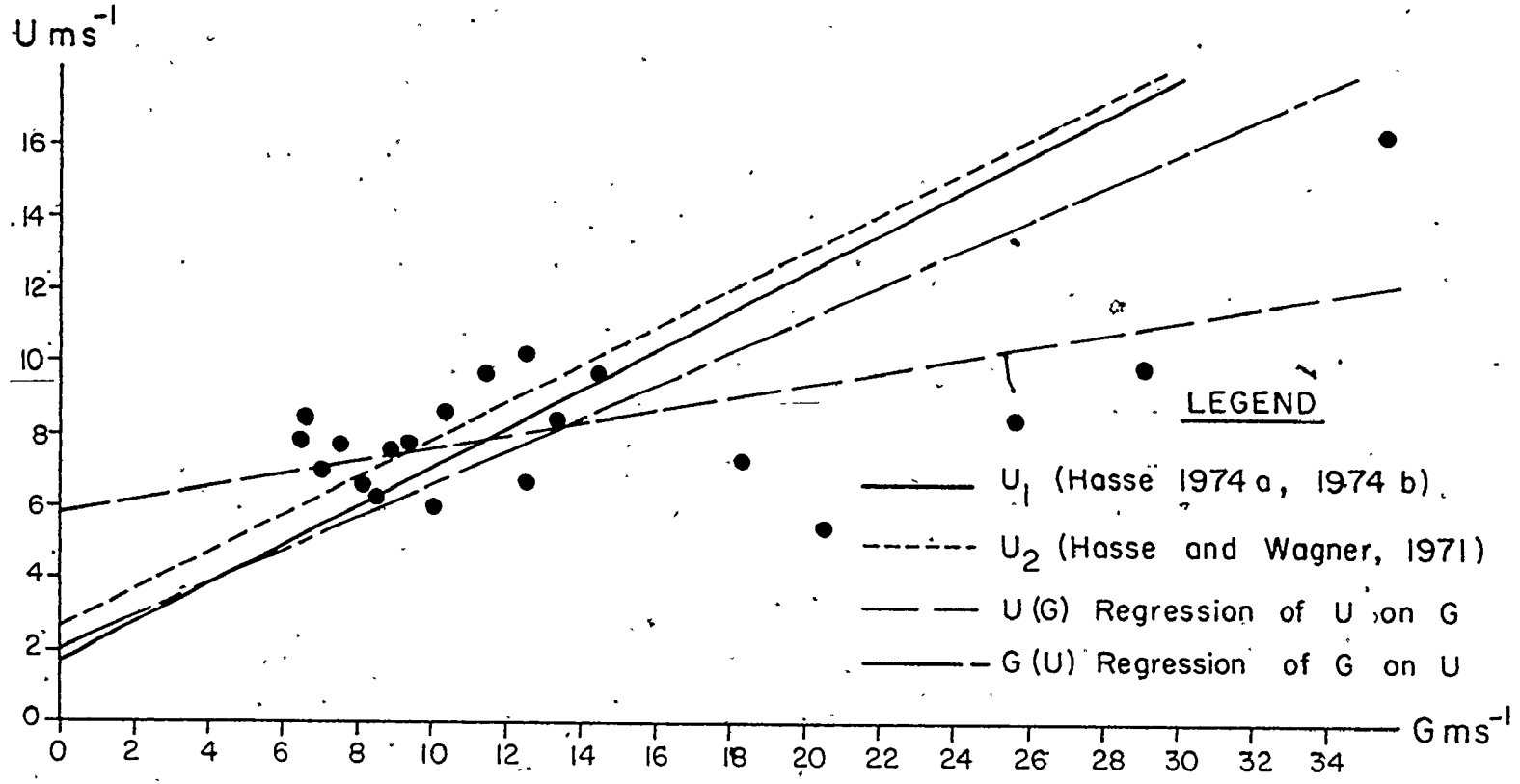

Figure K1 Site No. 2.

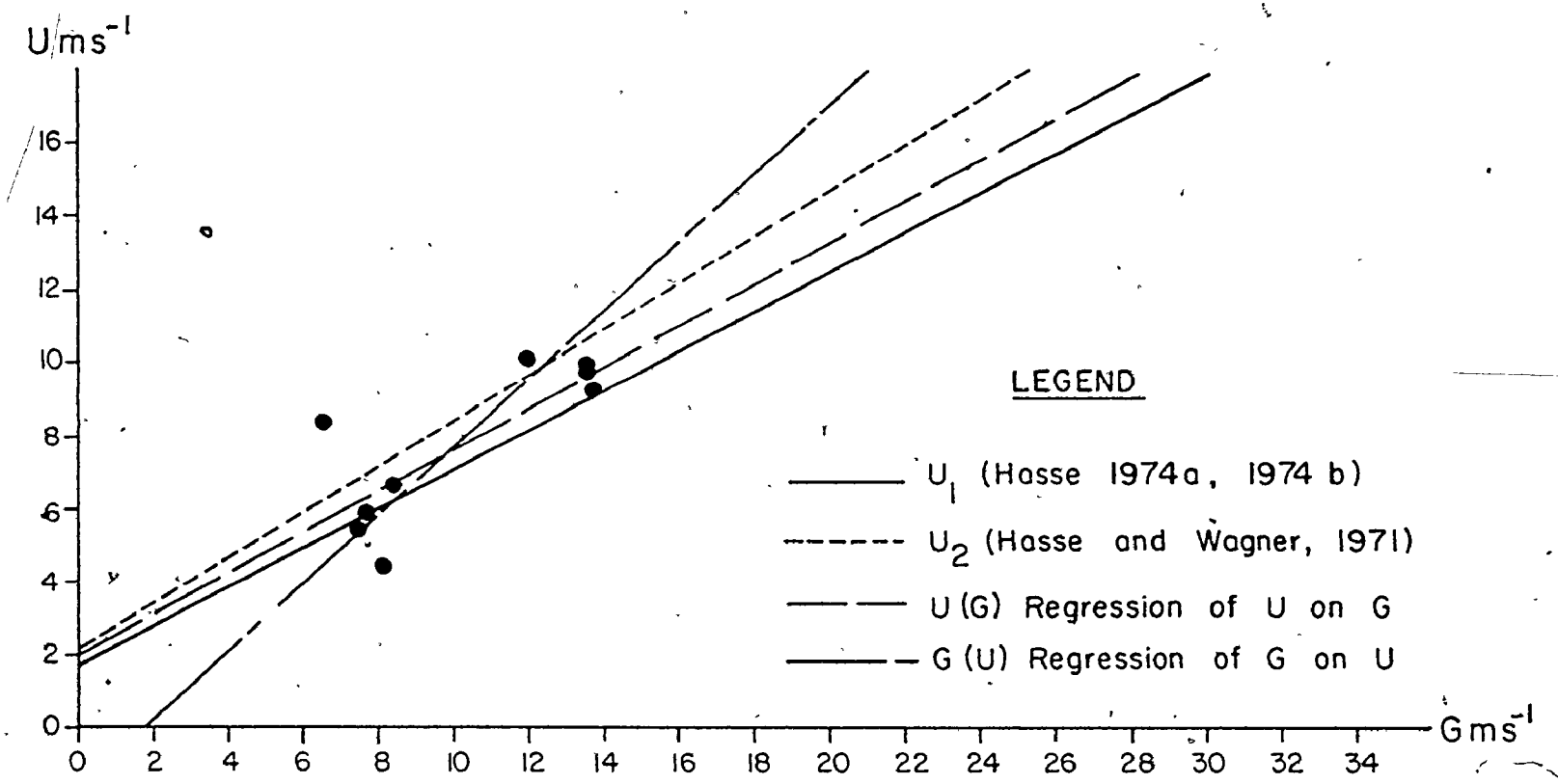

Figure K2 Site No. 4a

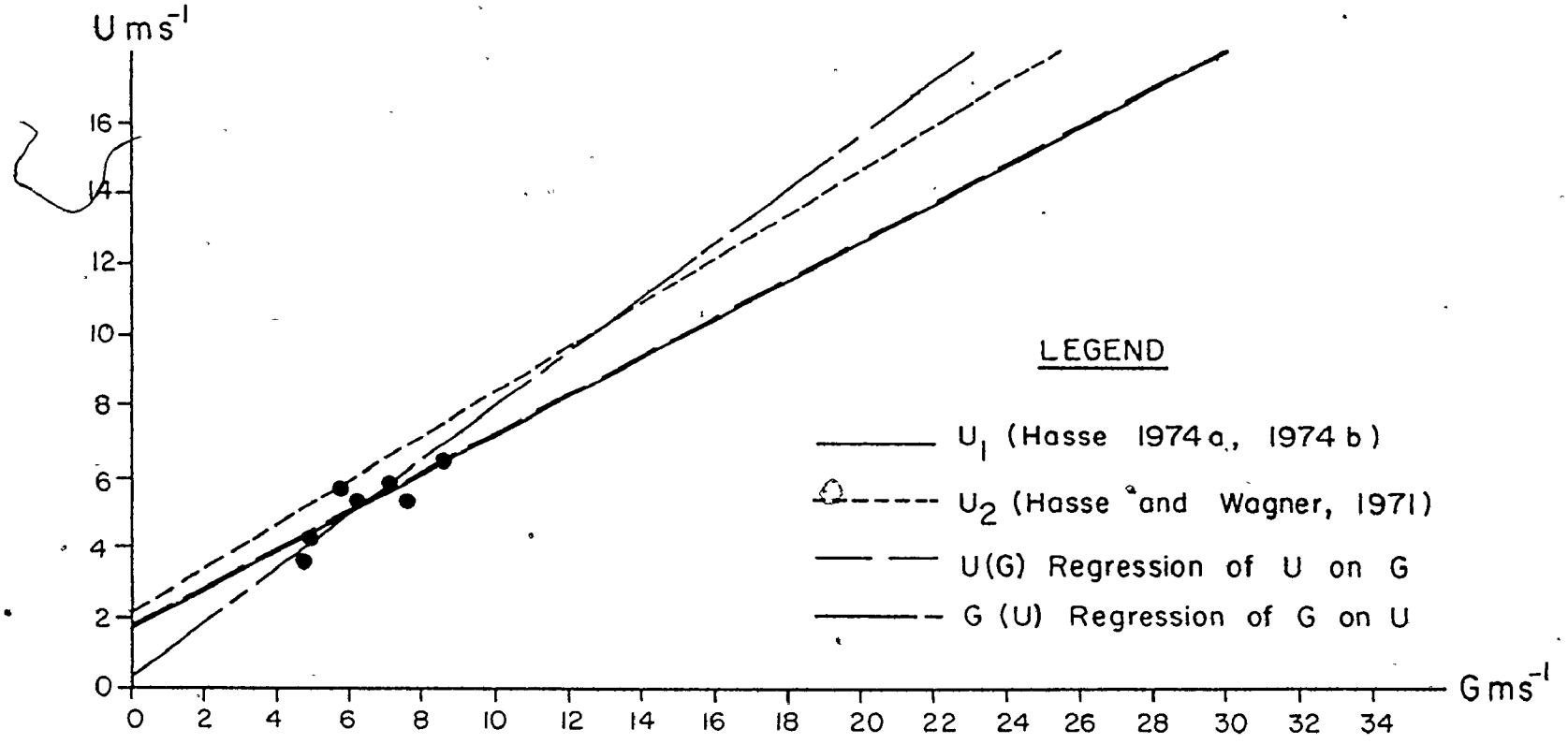

Figure K 3 Site No. 4 b

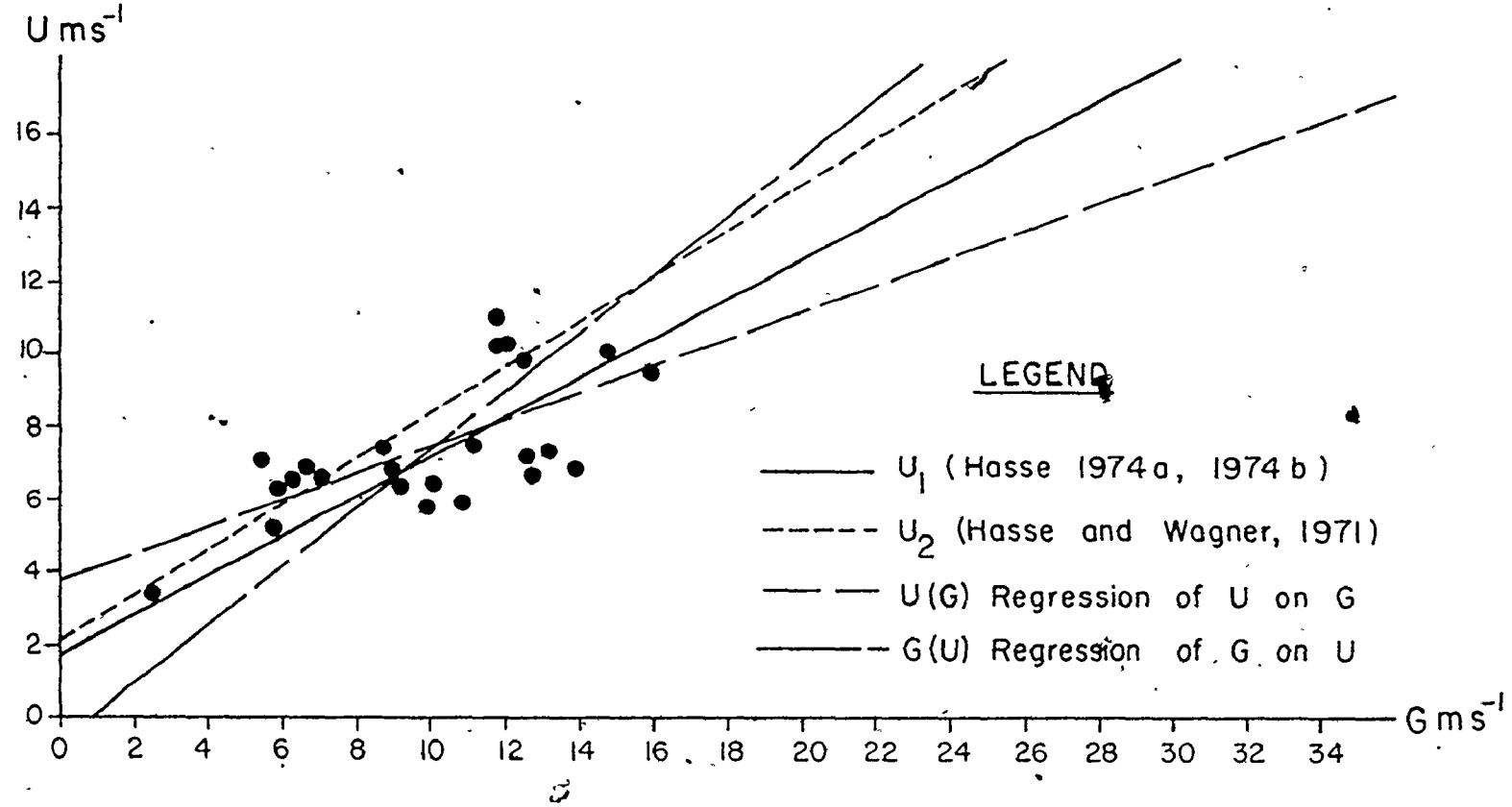

Figure K4 Site No. 5

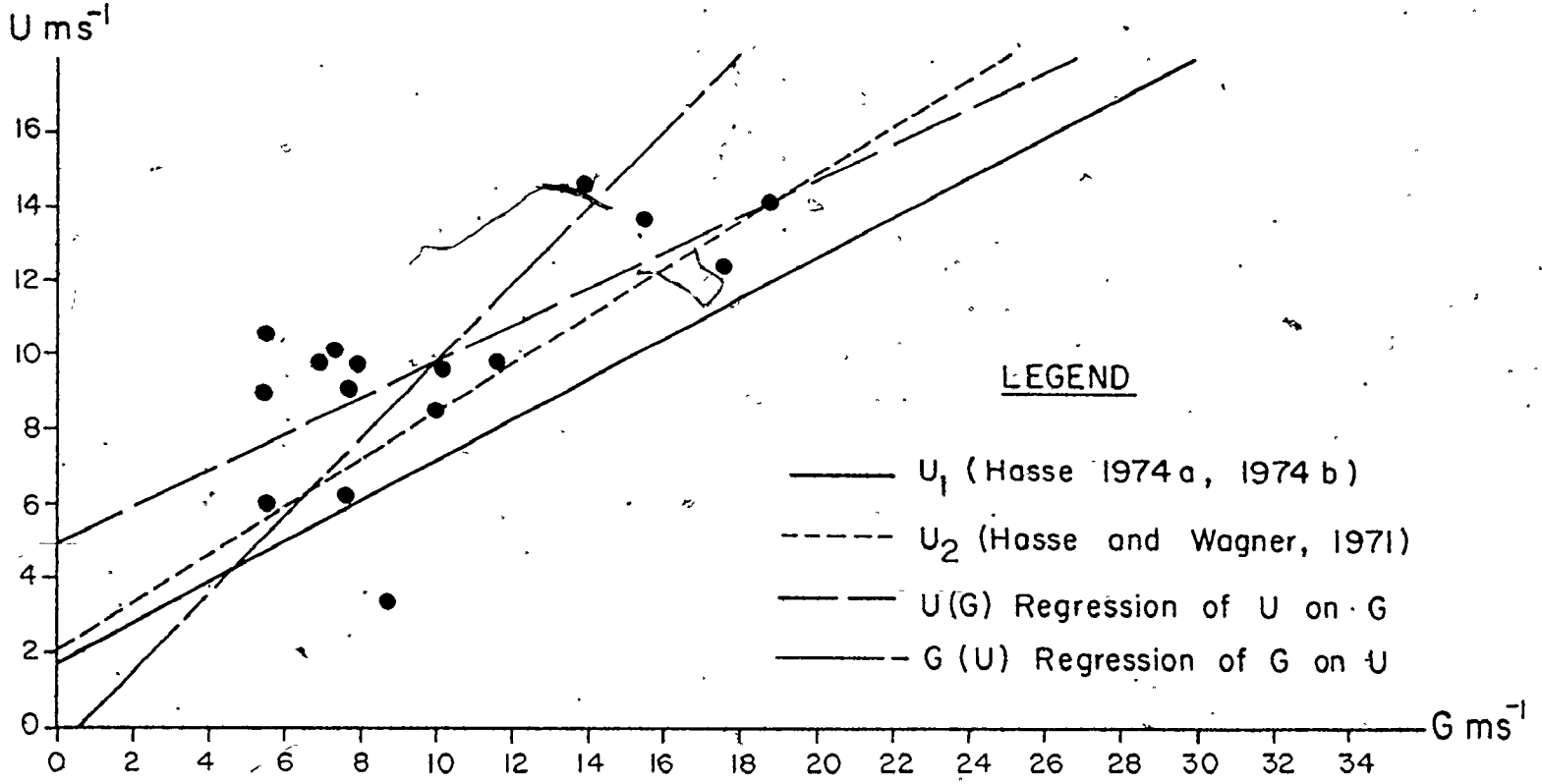

Figure K5 Site No. 6

REFERENCES

Aagaard, K., 1969: Relationship between geostrophic and surface winds at weather ship M. J. Geophy. Res., 74(13), 3440-3442.

AES, 1973: Ice thickness data for Canadian selected stations, freeze-up 1972 - break-up 1973. Atmospheric Environment Service, Canada, ICE 1-73, 37pp.

AES, 1974: Ice thickness data for Canadian selected stations, freeze-up 1973 - break-up 1974. Atmospheric Environment Service, Canada, ICE 1-74 46pp.

AES, 1975: Ice thickness data for Canadian selected stations freeze-up 1974 - break-up 1975. Atmospheric Environment Service, Canada, ICE 1-75 50pp.

AGS, 1975: World, 1:5,000,000, sheet 14, the Arctic region. American Geographical Society, New York.

Banke, E.G. and S.D. Smith, 1971: Wind stress over water in the Beaufort Sea. J. Geophy. Res., 76(30), 7368-7374.

Banke, E.G. and S.D. Smith, 1973: Wind stress on Arctic sea ice. J. Geophy. Res., 78(33), 7871-7883.

Brown, R.A., 1976: The resistance law. AIDJEX Bull. 31, 21-31.

Campbell, W.J., 1965: The wind driven circulation of ice and water in a Polar ocean. J. Geophy. Res., 70(14), 3279-3301.

CCRS, 1975: ERTS Imagery Catalogue. Cumulative Picture Centre Listing, May 1975. Canada Centre for Remote Sensing, 730pp.

Colvocresses, A.P., 1974: Space oblique mercator. Photogr. Eng., 40(8) 921-926.

Coon, M.D., 1977: A review of AIDJEX modeling. A Symposium on Sea Ice Processes and Models. Sept. 6-9, 1977, Seattle, Wash., Preprints 1, 40-55.

Crowder, W.K., H.L. McKim, S.F. Ackley, W.D. Hibler III and D.M. Anderson, 1973: Mesoscale deformation of sea ice from satellite imagery. Advanced Concepts and Techniques in the Study of Snow and Ice Resources. An Interdisciplinary Symposium. Dec. 2-6, 1973, Monterey, Cal., 563-573.

Dyer, A.J., and B.B. Hicks, 1970: Flux-gradient relationships in the constant flux layers. Quart. J. Roy. Meteor. Soc., 96, 715-721.

Dyer, A.J., 1974: A review of flux-profile relationships. Boundary Layer Meteor., 7, 363-372.

Fel'zenbaum, A.I., 1958: The theory of steady drift of ice and the calculation of the long period mean drift in the central part of the Arctic Basin. Problems of the North, 2, 13-44.

Gordon, A.H., 1952: The relationship between the mean vector surface wind and the mean pressure gradient over the oceans. Geofisica Pura e Applicata, 21, 49-51.

Hasse, L. and V. Wagner, 1971: On the relationship between geostrophic and surface wind at sea. Mon. Weather Rev., 99(4), 255-260.

Hasse, L., 1974a: Note on the surface to geostrophic wind relationship from observations in the German Bight. Boundary Layer Meteor., 6, 197-201.

Hasse, L., 1974b: On the surface to geostrophic wind relationship at sea and the stability dependence of the resistance law. Contrib. Atmos. Phys., 47, 45-55.

Hess, S.L., 1959: Introduction to Theoretical Meteorology. Holt, Rinhart and Winston, New-York, 362pp.

Hibler III, W.D., S.F. Ackley, W.K. Crowder, H.L. McKim and D.M. Anderson, 1974: Analysis of shear zone ice deformation in the Beaufort Sea using satellite imagery. The Coast and the Shelf of the Beaufort

Sea Symposium. Arctic Institute of North America. Arlington, Va., 285-296.

Johannessen, O.M., 1970: Note on some vertical current profiles below ice floes in the Gulf of St. Lawrence and near the North Pole. J. Geophys. Res., 75(15) 2857-2862.

Kratky, V., 1974: Cartographic accuracy of ERTS. Photogr. Eng., 40(2), 203-212.

Langleben, M.P., 1972: A study of the roughness parameter from wind profiles. J. Geophys. Res., 77(30), 5935-5944.

Langleben, M.P. and E.R. Pounder, 1975: On the air drag of an Arctic ice floe. Geophys. Res. Letters, 2(1), 15-18.

Lavrov, N.A., 1974: Analysis of experimental data on wind over the Baltic Sea. Meteor. and Hydrol., 10, 102-104.

Li, J.C.R., 1964: Statistical Inference I. Edwards Bros., Ann Arbor, 658pp.

Maykut, G.A., A.S. Thorndike and N. Untersteiner, 1972: AIDJEX scientific plan. AIDJEX Bull. 15, 1-67

McIntosh, D.H. and A.S. Thom, 1972: Essentials of Meteorology. Wykeham, London, 239pp.

McLain, E.P., 1972: Detection of ice conditions in the

Queen Elizabeth Islands. ERTS-1 Symposium, Sept. 29, 1972. NASA, No. X-650-73-10, 127-128.

McPhee, M.G. and J.D. Smith, 1975: Measurements of the turbulent boundary layer under pack ice. AIDJEX Bull. 29, 49-92.

Munro, D.S., 1975: Energy Exchange on a Melting Glacier. Ph.D. Thesis, McMaster Univ., Hamilton, 182pp.

Nansen, F., 1902: The Norwegian North Polar Expedition 1893-1896, Scientific Results, Vol. III Longmans, Green and Co., London, 357-386.

NASA, 1976: LANDSAT Data Users Handbook. National Aeronautics and Space Administration, No. 76SDS4258, Greenbelt, Md.,1v.

Neralla, V.R., W.S. Liu, S. Venkatesh and M.B, Danard, 1977: Technique for predicting sea ice. A Symposium on Sea Ice Processes and Models. Sept. 6-9. 1977, Seattle, Wash., Preprints 2, 87-97.

Nye, J.F. and D.R. Thomas, 1974: The use of satellite photographs to give the movement and deformation of sea ice. AIDJEX Bull. 27, 1-21.

Nye, J.F., 1975: The use of ERTS photographs to measure the movement and deformation of sea ice. J. Glaciol.,15 (73), 429-436.

Post, L.A., 1954: A practical method for the prediction of the surface currents of the ocean. Tellus, 6 (1),59-62.

Pounder, E.R., 1965: The Physics of Ice. Pergamon, Oxford, 151pp.

Reed, R.J. and W.J. Campbell, 1962: The equilibrium drift of ice station Alpha. J. Geophys. Res., 67(1), 281-297.

Reeves, R.G. ed., 1975: Manual of Remote Sensing. Amer. Soc. Photogr., Falls Church, Va., 2v., 2144pp.

Reynolds, G., 1956: A wind analysis for the Northern Irish Sea. Quart. J. Roy. Meteor. Soc., 82, 469-480.

Roll, H.U., 1965: Physics of the Marine Atmosphere. Academic Press, New York, 426pp.

Rossby, C.G. and R.B. Montgomery, 1935: The layer of frictional influence in wind and water currents, Papers Phys. Oceanog. and Meteor., Mass. Inst. Technol. and Woods Hole Oceanog. Inst., 3, 1-100.

Seifert, W.J. and M.P. Langleben, 1972: Air drag coefficient and roughness length of a cover of sea ice. J. Geophys. Res., 77(15), 2708-2713.

Shuleikin, V.V., 1938: The drift of ice fields. Contes Rendus (Doklady), Acad. Sci. USSR, 19(8), 589-594.

Smith, S.D., E.G. Banke, and O.M. Johannessen, 1970: Wind stress and turbulence over ice in the Gulf of St. Lawrence. J. Geophys. Res., 75(15), 2803-2812.

Smith, S.D., 1972: Wind stress and turbulence over a flat ice floe. J. Geophys. Res., 77(21), 3886-3901.

Sobczak, L.W., 1977: Ice movements in the Beaufort Sea 1973-1975: determination by ERTS imagery. J. Geophys. Res. 82(9) 1413-1418.

Sverdrup, H.U., 1928: The wind-drift of ice on the North Siberian Shelf. The Norwegian North Polar Expedition with the "Maud" 1918-1925, Scientific Results, 4, 1-46.

Thorndike, A.S., 1973: An integrated system for measuring ice motions. Ocean 73: IEEE International Conference of Engineering in the Ocean Environment, IEEE, New York, 490-499.

Untersteiner, N. and F.I. Badgley, 1965: The roughness parameter of sea ice. J. Geophys. Res., 70(18), 4573-4577.

Untersteiner, N., 1977: AIDJEX review. A Symposium on Sea Ice Processes and Models. Sept. 6-9, 1977, Seattle Wash., Preprints 1, 2-9.

Wendler, G. and K.O.L.F. Jayaweera, 1974: Technique to obtain ice movement. J. Geophys. Res., 79(24),

3478-3479.

Williams, E., C. Swithinbank and G. de Robin, 1975: A submarine sonar study of Arctic pack ice, J. Glaciol., 15(73), 349-362.

WMO, 1972: WMO Sea Ice Nomenclature. World Meteorological Organization, Geneva, 147pp.

Wu, J., 1972: Note on the surface roughness and resistance coefficient of sea ice. J. Geophys. Res., 77(18), 3272-3277.